IKR Publishers

IKR Journal of Engineering and Technology (IKRJET)
Journal homepage: https://ikrpublishers.com/ikrjet/
Volume-2, Issue-3 (May-June) 2026

OPEN ACCESS
ISSN: 3107-7331 (Online)

Improving Filterability of Hydroxide Precipitates in Hydrometallurgical Hydrolysis Processes: A Critical Review

Antonio Clareti Pereira *
PhD in Chemical Engineering São Paulo University – USP Belo Horizonte – MG – Brazil

DOI:*10.5281/zenodo.20098962*

ARTICLE INFO

Article history:
Received : 01-05-2026
Accepted : 05-05-2026
Available online : 09-05-2026

Citation: Pereira, A. C. (2026). Improving Filterability of Hydroxide Precipitates in Hydrometallurgical Hydrolysis Processes: A Critical Review. *IKR Journal of Engineering and Technology (IKRJET), 2*(3), 21-45.

ABSTRACT **Original Research Article**

Hydrolysis-based precipitation is widely used in hydrometallurgy for impurity removal and metal recovery; however, the resulting hydroxide precipitates frequently exhibit poor filterability, leading to low filtration rates, high cake moisture, and significant operational constraints. Despite extensive research on precipitation chemistry, the link between formation mechanisms and solid–liquid separation performance remains insufficiently addressed. This review critically examines how supersaturation, nucleation and growth kinetics, solution chemistry, and hydrodynamic conditions govern the evolution of hydroxide structure—from primary particles to aggregated networks—and ultimately determine cake permeability and compressibility. Evidence from both laboratory and industrial systems shows that filterability is not an intrinsic property of the solid but a consequence of its formation history and structural organization. Strategies such as controlled supersaturation, seeded precipitation, temperature optimization, and selective flocculation are evaluated, highlighting trade-offs between filtration performance, product purity, and process stability. The review identifies key gaps, including the lack of standardized metrics, limited coupling between precipitation and filtration studies, and insufficient scale-up validation. A process-integrated framework is proposed to connect reaction pathways with filtration behavior, providing a basis for designing hydrolysis systems with improved solid–liquid separation performance.

Keywords: Hydrometallurgy, Hydrolysis, Hydroxide Precipitation, Filterability, Solid–Liquid Separation, Cake Permeability.

Highlights

- Hydroxide filterability depends on formation history, not intrinsic particle size
- Supersaturation control governs structure, permeability, and filtration performance
- Precipitation and filtration are strongly coupled but often treated independently
- Process-integrated design is essential to improve industrial solid–liquid separation.

Graphical Abstract

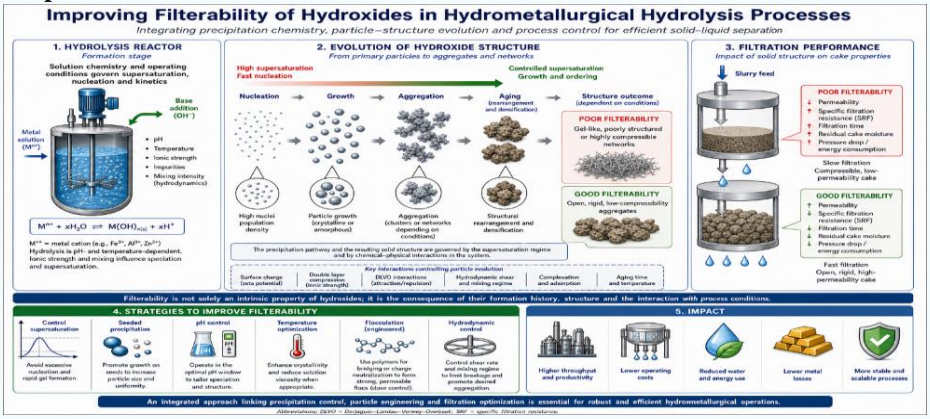

*Corresponding author: Antonio Clareti Pereira
PhD in Chemical Engineering São Paulo University – USP Belo Horizonte – MG – Brazil

Introduction

Hydrolysis-based precipitation is a cornerstone of hydrometallurgical processing. It is widely used for impurity removal and, in some cases, for selective metal recovery from aqueous solutions (Binnemans et al., 2020; Deblonde et al., 2023; Faris et al., 2021). The approach is attractive for its simplicity, low reagent costs, and compatibility with large-scale operations. Typical applications include removing iron and aluminum, separating rare earths, and purification steps in base metal circuits (Hedwig et al., 2023; Jenssen et al., 2021). In practice, hydrolysis is often treated as a purely chemical operation, with performance evaluated primarily by precipitation efficiency and selectivity.

This perspective is incomplete. A recurring issue in industrial systems is the formation of poorly filterable hydroxide precipitates (Dobre et al., 2024; Siddig et al., 2024). These solids often display colloidal or gel-like behavior. They form fine, highly hydrated networks rather than discrete, well-defined particles. Consequently, downstream solid–liquid separation becomes the limiting step, not the precipitation reaction itself.

The consequences are well known yet still underestimated. Low permeability of the filter cake reduces filtration rates and constrains plant throughput (Barros et al., 2025). High moisture retention increases drying requirements and causes metal losses in the retained liquor (Dittmer et al., 2025). Filter media clogging and rapid pressure build-up further compromise operational stability. In extreme cases, the filtration unit dictates overall plant capacity. These effects are routinely reported in practice, yet they are rarely addressed in precipitation design.

The root of the problem lies in how hydroxides form and evolve. Rapid nucleation under high supersaturation tends to generate very fine primary particles (Dobre et al., 2024). These particles can aggregate into dense or gel-like structures with poor drainage characteristics. In systems containing aluminum, iron, or silica, polymerization and network formation can dominate (Deblonde et al., 2023; Hedwig et al., 2023). The resulting solids exhibit high compressibility and low permeability. Importantly, these properties are not fixed. They depend strongly on solution chemistry, mixing conditions, and time-dependent structural rearrangement (Faris et al., 2021).

Despite this, most studies remain focused on chemical yield. Precipitation is typically optimized to maximize metal removal or recovery (Binnemans et al., 2020; Jenssen et al., 2021). Filtration behavior is treated as a secondary constraint, often addressed ex post through flocculants or equipment changes. This separation between reaction design and solid–liquid separation is a fundamental limitation in the current literature (Siddig et al., 2024). It prevents a mechanistic understanding of why certain precipitates filter well while others do not.

Another limitation is the reliance on simplified descriptors such as particle size distribution. While particle size is relevant, it does not capture the internal structure of aggregates, their porosity, or their response to compression (Barros et al., 2025). Two precipitates with similar size distributions can exhibit markedly different filtration behavior. Structural features such as fractal dimension, degree of aggregation, and pore connectivity are rarely quantified, yet they control cake permeability and resistance (Dittmer et al., 2025).

This review takes a different approach. It treats hydrolysis and filtration as intrinsically coupled processes. The central premise is that filterability is not an intrinsic property of hydroxide precipitates. It is the outcome of their formation history and structural evolution. Nucleation, growth, aggregation, and aging must be considered as a continuum that defines the final cake structure (Dobre et al., 2024; Faris et al., 2021).

This article critically analyzes the relationships among precipitation conditions, particle structure, and filtration performance in hydrometallurgical hydrolysis systems. It emphasizes identifying the mechanisms that govern the transition from dispersed particles to filter cakes with distinct permeability and compressibility. Process strategies to improve filterability are evaluated for their underlying physicochemical basis and trade-offs with product quality and process stability. Finally, key gaps in the current literature are highlighted, with a focus on the need for integrated approaches linking reaction engineering and solid–liquid separation design.

Methodology

This review adheres to the Preferred Reporting Items for Systematic Reviews and Meta-Analyses (PRISMA 2020) framework to ensure transparency, reproducibility, and methodological rigor in identifying, screening, and synthesizing the literature (Page et al., 2021). The methodology was designed to capture both fundamental and applied studies on hydroxide precipitation and its effects on solid–liquid separation performance in hydrometallurgical systems.

The literature search was conducted using Scopus, Web of Science, and ScienceDirect, covering 2000–2026, with an emphasis on recent developments (2015–2026). Search strings combined three core domains: (i) hydrolysis/precipitation, (ii) structure/aggregation, and (iii)

filtration/solid–liquid separation. Representative queries included: "hydroxide precipitation AND filterability", "metal hydrolysis AND cake permeability", and "aggregation AND filtration performance hydrometallurgy". The initial search returned approximately 1,150–1,300 records, depending on database overlap.

After removing duplicates (≈25–30%), titles and abstracts were screened for relevance to: (i) hydroxide precipitation mechanisms, (ii) particle aggregation and structure, and (iii) filtration or dewatering performance. Studies focused solely on precipitation yield, without structural or separation analysis, were excluded at this stage. The screening process reduced the dataset to approximately 400–500 records.

Full-text assessment was then conducted using stricter eligibility criteria. Included studies were required to report at least one of the following: (i) filtration parameters (e.g., specific cake resistance typically in the range of 10^{10}–10^{13} m/kg), (ii) structural descriptors (e.g., particle size, porosity, or aggregation behavior), or (iii) process variables directly influencing filterability (e.g., pH typically 3–7 for Fe/Al systems, temperature 25–90 °C, ionic strength 0.01–1.0 M). Studies lacking experimental validation or presenting purely qualitative observations without measurable parameters were excluded. This step yielded a final dataset of 112 references, which forms the basis of this review.

The analysis used a process-integrated approach, grouping the literature into four interconnected domains: (i) precipitation chemistry and kinetics, (ii) particle structure and aggregation, (iii) cake formation and filtration behavior, and (iv) process strategies to improve filterability. This structure reflects the review's central premise that precipitation and solid–liquid separation must be analyzed as a coupled system.

The workflow for the literature selection is summarized in Figure 1. The PRISMA 2020 flow diagram for the literature selection process used in this review details the identification, screening, eligibility, and inclusion stages.

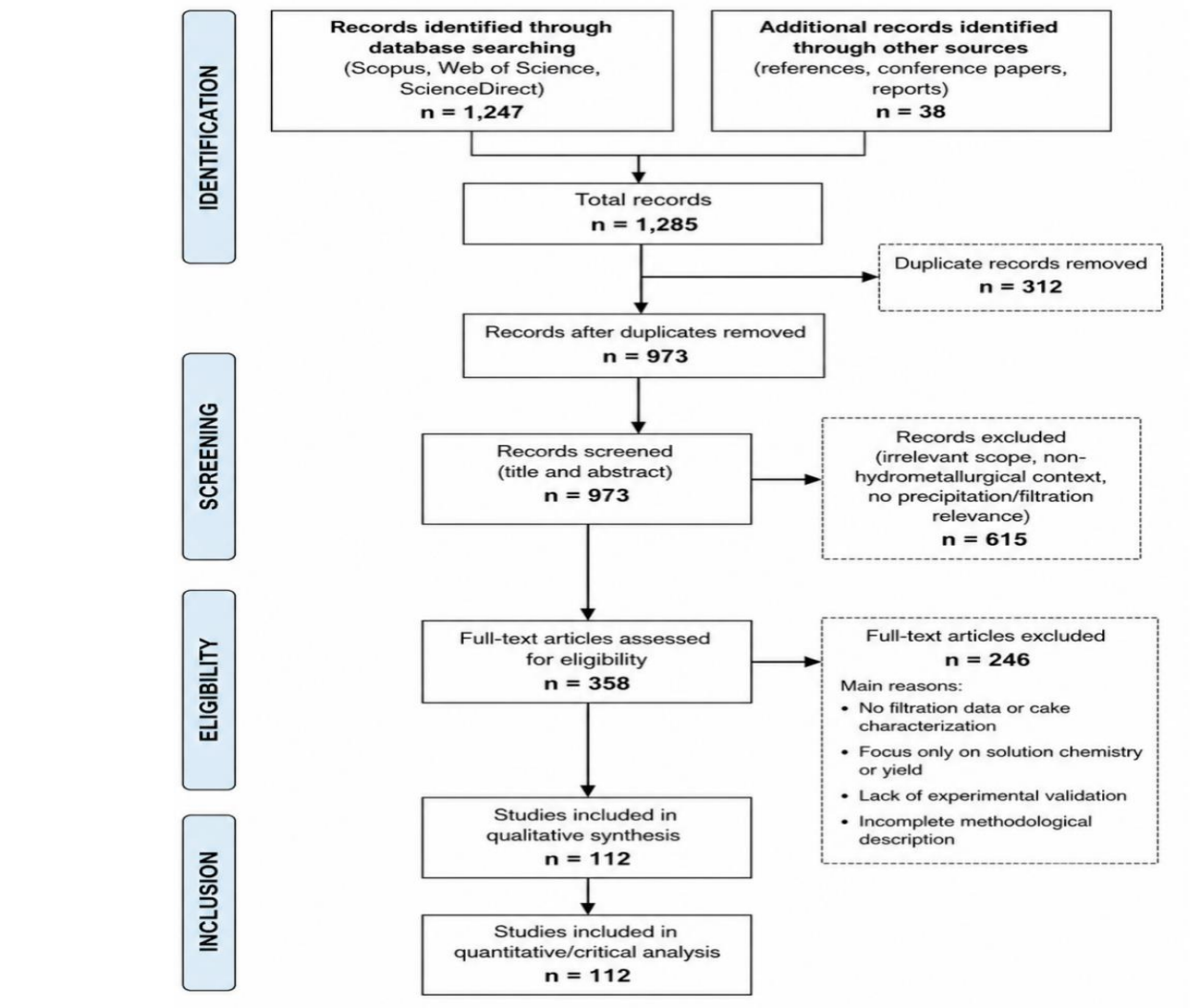

Figure 1. PRISMA 2020 flow diagram of the literature selection process used in this review, including identification, screening, eligibility, and inclusion stages. Adapted from Page et al. (2021).

Figure 1 shows the progressive reduction from the initial dataset to the final corpus of 112 studies. A substantial share of excluded records lacked quantitative filtration data or any description of cake structure. In practical terms, more than 50% of screened studies focused exclusively on precipitation yield or solution chemistry. This imbalance underscores a

structural limitation in the literature. Precipitation is often optimized in isolation, while filtration performance is treated as an operational constraint rather than a design variable. This methodological gap directly supports the need for integrated experimental approaches that evaluate precipitation conditions and solid–liquid separation metrics simultaneously.

Fundamentals of Hydroxide Formation in Hydrolysis

Hydrolysis Reactions

Hydrolysis of metal ions in aqueous systems proceeds via stepwise deprotonation, forming hydroxo-complexes before precipitation. In hydrometallurgy, the most relevant ions are Fe^{3+}, Al^{3+}, REE^{3+}, and Zn^{2+}, each with distinct hydrolysis constants and stability fields (Chen et al., 2020; Faris et al., 2021). These reactions are governed by pH, temperature, ionic strength, and complexing species, which determine both equilibrium and kinetic pathways.

For Fe^{3+} and Al^{3+}, hydrolysis begins at low pH and proceeds rapidly. Bulk precipitation typically occurs at pH 2.5–4.5 for Fe^{3+} and 4.5–6.5 for Al^{3+}, though sulfate and chloride ions can shift these thresholds. REE^{3+} precipitation generally requires pH 6–8, reflecting weaker hydrolysis tendencies. Zn^{2+} remains soluble until pH 7–9, when $Zn(OH)_2$ forms with slower kinetics (Balinski et al., 2020; Emil-Kaya et al., 2023).

Supersaturation is the primary driver of precipitation. In industrial systems, local supersaturation often exceeds equilibrium by 10–100× due to imperfect mixing. This leads to rapid nucleation and the formation of highly dispersed solids. Hydrolysis reaction times are typically short (seconds to minutes), whereas structural evolution continues over longer timescales (minutes to hours). This temporal mismatch is rarely considered in reactor design.

To provide a quantitative overview, Table 1, Typical hydrolysis conditions and precipitation characteristics of key metal ions, summarizes the key physicochemical parameters relevant to hydroxide formation.

Table 1. Typical hydrolysis conditions and precipitation characteristics of key metal ions in hydrometallurgical systems, including pH range, dominant species, and structural tendencies. Adapted from Chen et al. (2020), Faris et al. (2021), and Emil-Kaya et al. (2023).

Metal ion	Typical precipitation pH	Dominant species before precipitation	Kinetic behavior	Structural tendency
Fe^{3+}	2.5–4.5	$Fe(OH)^{2+}$, $Fe(OH)_2^{+}$	Very fast	Amorphous/gel-like
Al^{3+}	4.5–6.5	$Al(OH)^{2+}$, $Al(OH)_2^{+}$	Fast	Polymeric/gel-like
REE^{3+}	6–8	$REE(OH)^{2+}$	Moderate	Crystalline/amorphous
Zn^{2+}	7–9	$Zn(OH)^{+}$	Slower	More crystalline

Table 1 shows that metals with high charge density (Fe^{3+}, Al^{3+}) tend to form amorphous or polymeric structures under typical process conditions. In contrast, divalent ions such as Zn^{2+} favor more crystalline precipitates. This distinction has direct implications for downstream filtration.

Nucleation vs Growth

The balance between nucleation and growth determines particle size and initial structure. At high supersaturation, nucleation dominates, yielding particles typically below 1 µm. These particles have high surface energy and a strong tendency to aggregate. At lower supersaturation, growth dominates, producing larger particles in the range of 5–50 µm, depending on residence time and temperature (Lin et al., 2021; Liao et al., 2024).

In practice, supersaturation is not uniform. Reagent addition and mixing generate local gradients, resulting in simultaneous nucleation and growth. This produces broad particle size distributions and heterogeneous structures. Such heterogeneity is a key factor in filtration but is rarely quantified.

Classical models, such as the LaMer framework, assume a clear separation between nucleation and growth. This assumption does not hold in continuous or semi-batch hydrometallurgical reactors. Continuous addition of neutralizing agents sustains nucleation over time. More importantly, these models neglect aggregation dynamics, which dominate as solids concentration increases (Zhu et al., 2022).

From a design perspective, reducing supersaturation through staged neutralization or controlled dosing can promote growth. However, this approach requires longer residence times (30–120 min) and larger reactor volumes. This trade-off between particle size and capital cost is often overlooked.

Polymerization and Gel Formation

Polymerization is critical in systems containing Fe^{3+} and Al^{3+}. Hydrolyzed species can form polynuclear complexes that evolve into extended networks. This results in amorphous, highly hydrated structures commonly described as gels (Deng et al., 2021; Wang et al., 2022).

Gel formation typically occurs near the precipitation threshold, where partially hydrolyzed species coexist with solids. Under these conditions, the system transitions from discrete particles to a continuous network. Water content in these structures can reach 70–90 wt%, resulting in extremely low permeability and high compressibility (Han et al., 2024).

The presence of impurities strongly influences this behavior. Silica is particularly critical, as it promotes the formation of

mixed silicate–hydroxide gels. These structures are more resistant to dewatering and often require chemical conditioning.

A key limitation of current models is their neglect of time-dependent evolution. After precipitation, solids undergo aging processes such as densification and partial crystallization. These changes can improve filterability, but they require time scales often longer than industrial residence times. As a result, many systems operate with metastable, poorly structured solids.

The sequence of hydroxide formation mechanisms is summarized in Figure 2. The conceptual scheme of hydroxide formation during hydrolysis illustrates the transition from dissolved species to structured aggregates and gels.

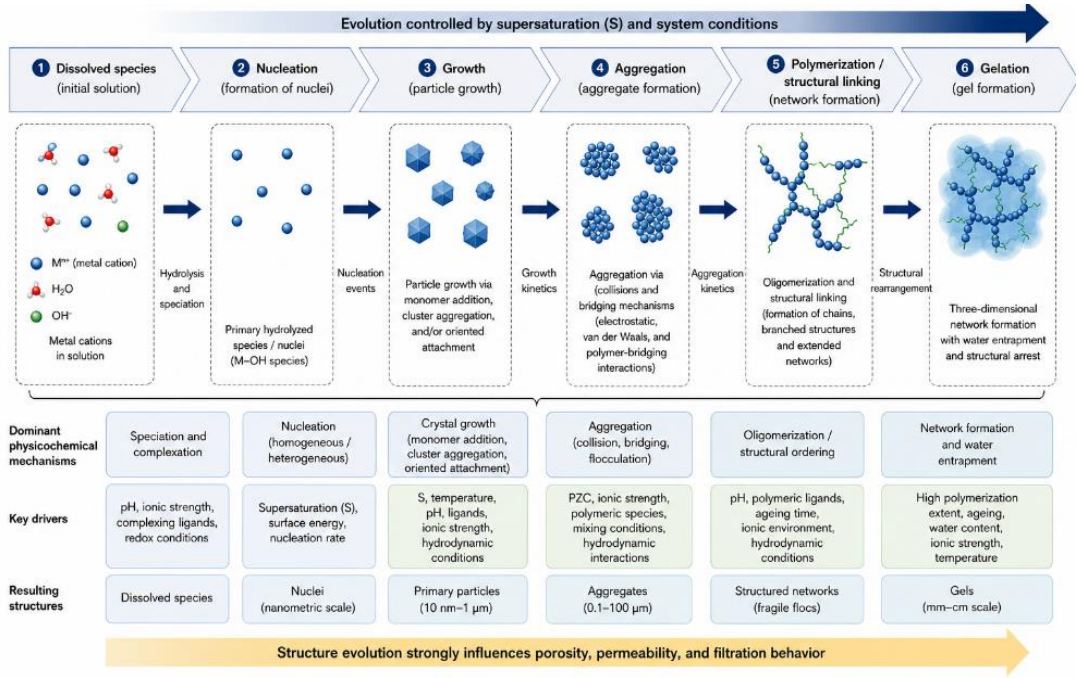

Figure 2. Conceptual scheme of hydroxide formation during hydrolysis, illustrating the interplay between supersaturation, nucleation, growth, aggregation, and polymerization leading to distinct particle structures. Adapted from Zhu et al. (2022) and Deng et al. (2021).

Figure 2 highlights that hydroxide formation is governed by coupled mechanisms rather than isolated steps. The transition from particles to aggregates and gels defines the internal structure of the solids. This structure, rather than particle size alone, controls permeability and filtration behavior. The lack of integration between formation mechanisms and separation performance remains a central limitation in current hydrometallurgical practice.

Definition and Metrics of Filterability

Filterability is the ability of a suspension to form a permeable cake that allows liquid flow under an applied pressure gradient. In hydrometallurgical systems, it is a process-limiting property. It directly affects filtration rate, cake moisture, and equipment sizing. Typical industrial filtration fluxes range from 50 to 500 $L \cdot m^{-2} \cdot h^{-1}$, depending on cake structure and operating pressure (Audet et al., 2022; Guo et al., 2022). Poorly filterable hydroxides often operate at the lower end of this range, increasing CAPEX because larger filter areas are required.

Key Parameters

Filterability is quantified using a set of interrelated parameters that describe cake structure and flow resistance (Gafiullina et al., 2020; Fan et al., 2026).

- Specific cake resistance (α) [m/kg]:
  Measures resistance to flow per unit mass, with typical hydroxide values from 10^{10} to 10^{13} m/kg, reaching gel-like precipitates at the upper end.
- Permeability (k) [m²]:
  Describes fluid flow through the cake, with values typically from 10^{-14} to 10^{-11} m².
- Porosity (ε) [-]:
  Fraction of void volume. Hydroxide cakes often exhibit ε = 0.6–0.9, but high porosity does not necessarily imply high permeability due to pore connectivity.
- Compressibility index (s) [-]:
  Defines how α varies with pressure. Highly compressible cakes (s ≈ 0.5–1.0) exhibit a strong reduction in permeability under pressure.

To consolidate these parameters, Table 2, Key filterability parameters and typical ranges for hydroxide precipitates, summarizes their definitions and industrial relevance.

Table 2. Key filterability parameters and typical ranges for hydroxide precipitates in hydrometallurgical systems, including definitions, units, and operational implications. Adapted from Audet et al. (2022) and Guo et al. (2022).

Parameter	Symbol	Typical range	Unit	Operational implication
Specific cake resistance	α	10^{10}–10^{13}	m/kg	Controls filtration rate
Permeability	k	10^{-14}–10^{-11}	m²	Governs fluid flow
Porosity	ε	0.6–0.9	–	Indicates void fraction
Compressibility	s	0.2–1.0	–	Affects pressure response

Table 2 shows that high porosity does not necessarily imply high permeability. In many hydroxide systems, the pore structure is poorly connected, leading to high resistance despite a high void fraction. This distinction is critical for interpreting filtration data.

Classical Filtration Models

Filtration behavior is commonly described using Darcy's law and its extensions. For incompressible cakes, the filtration rate is given by Equation 1:

$$\frac{dV}{dt} = \frac{\Delta P}{\mu(R_m + \alpha C V)} \quad \text{Equation 1}$$

where ΔP is pressure drop, μ is viscosity, R_m is medium resistance, and C is solids concentration (Audet et al., 2022).

The Kozeny–Carman equation establishes a relationship between permeability and the structural properties of porous media:

$$k = \frac{\varepsilon^3}{K(1-\varepsilon)^2 S^2} \quad \text{Equation 2}$$

where S is specific surface area, and K is a constant (Raponi et al., 2025).

These models provide a useful framework for interpreting filtration data, estimating cake resistance, and scaling filtration equipment. In industrial practice, filtration pressures typically range from 1 to 7 bar, depending on equipment type (pressure vs vacuum filters).

The relationship between structure and filtration behavior is illustrated in Figure 3. This relationship links cake structure to filtration performance and connects particle size, porosity, and permeability.

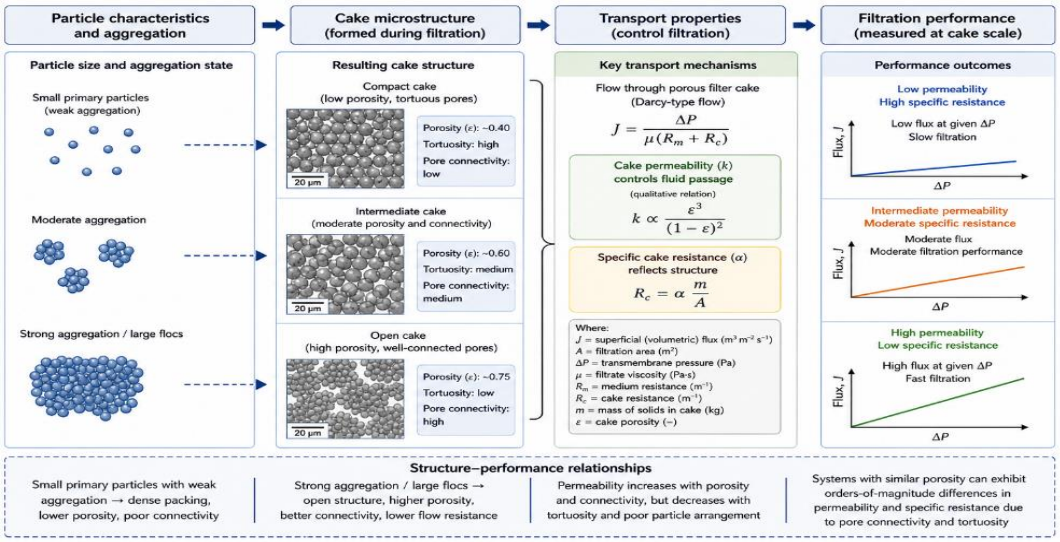

Figure 3. Relationship between cake structure and filtration performance, showing the influence of particle size, porosity, and aggregation on permeability and specific resistance. Adapted from Raponi et al. (2025).

Figure 3 highlights that permeability is controlled not only by porosity but also by pore connectivity and particle arrangement. Systems with similar porosity can exhibit orders-of-magnitude differences in permeability.

Limitations of Current Metrics and Models

Despite their widespread use, classical models have important limitations. They assume homogeneous, isotropic media with constant structure. These assumptions do not hold for hydroxide precipitates.

Hydroxide cakes are heterogeneous and evolve dynamically, with aggregation, restructuring, and compression during filtration. Increased pressure causes pore collapse, reducing permeability, which isn't reflected by constant α or k values (Jenssen et al., 2021; Siddig et al., 2024).

Another limitation is the neglect of flocculation dynamics. In many systems, particle aggregation continues during filtration, altering the cake structure in real time. Similarly, structural collapse under pressure leads to nonlinear filtration behavior. These effects are particularly pronounced in gel-like systems.

A critical issue is the overreliance on particle size distribution (PSD) as a predictor of filterability. Although PSD influences

permeability, it does not capture aggregate structure or pore connectivity. Two systems with similar PSD can differ by one to two orders of magnitude in α (Barros et al., 2025; Dittmer et al., 2025).

The central limitation can be summarized as follows:
→filterability is a structural property, not a size-based property**.**

This limitation explains why many precipitation processes optimized for particle size still exhibit poor filtration performance. It also reinforces the need to link precipitation mechanisms with structural descriptors, rather than relying solely on classical filtration metrics.

The next section examines the physicochemical factors that control these structural properties and, consequently, filterability in hydrometallurgical systems.

Physicochemical Factors Controlling Filterability

Filterability is highly sensitive to the chemical environment during precipitation. Small variations in solution chemistry can shift the system from well-drained particulate cakes to gel-like, poorly permeable structures. This section examines the main physicochemical variables controlling this transition and quantifies their operational impact.

pH and Supersaturation

pH directly controls the extent of hydrolysis and supersaturation. It determines both the onset of precipitation and the dominant formation mechanism. At low supersaturation, particle growth dominates. At high supersaturation, nucleation prevails, producing fine particles with high specific resistance (Fu et al., 2025; Lin et al., 2021).

In practical systems, supersaturation ratios ($S = C/C^*$) can reach 10–100, particularly during rapid neutralization. Under these conditions, particle sizes typically fall below 1 µm, and aggregation becomes dominant. Near the precipitation threshold, a critical gelation zone is often observed. For Fe^{3+} and Al^{3+} systems, this zone typically occurs within ±0.5 pH units of the precipitation pH (Song et al., 2021; Ibrahim et al., 2025).

Operating outside this narrow window is essential. Even a slight pH overshoot can trigger polymerization and gel formation, yielding α values above 10^{12} m/kg. Controlled pH adjustment via staged neutralization can reduce supersaturation and shift the system toward growth-dominated regimes (Amadghous et al., 2025).

Temperature

Temperature affects both reaction kinetics and fluid properties. Increasing temperature accelerates hydrolysis and enhances crystal growth rates. For many hydroxide systems, raising the temperature from 25 °C to 70–90 °C increases particle size by a factor of 2–5, depending on residence time (Arampatzis et al., 2025; Liu et al., 2025).

Temperature also reduces solution viscosity. Water viscosity decreases from ~0.89 mPa·s at 25 °C to ~0.32 mPa·s at 90 °C, directly improving filtration rates. In Darcy's regime, this can increase filtration flux by 2–3×, assuming a constant cake structure (Tang et al., 2026).

However, higher temperatures increase energy demand. Heating slurry streams from ambient to 80 °C typically requires ~200–300 kWh per m^3, depending on the level of heat recovery. This creates a trade-off between improved filterability and operating costs.

Ionic Strength and Electrolytes

Ionic strength governs interparticle interactions by compressing the electrical double layer. At low ionic strength (<0.01 M), particles remain dispersed because of electrostatic repulsion. At higher ionic strength (0.1–1.0 M), charge screening promotes aggregation (Deng et al., 2021; Kalaitzidou et al., 2022).

This transition is critical for filtration. Aggregated structures typically exhibit higher permeability due to improved pore connectivity. However, excessive aggregation can form dense clusters with low internal porosity. The optimal ionic strength range is system-specific but often falls between 0.05 and 0.5 M (Arrisujaya et al., 2025).

Electrolyte type also matters. Multivalent ions (e.g., Ca^{2+}, Mg^{2+}) are more effective at destabilizing colloids than monovalent ions. Their presence can significantly reduce α, often by one order of magnitude.

Impurities

Impurities play a decisive role in determining structure and filterability, with silica being the most critical. Dissolved silica can polymerize and interact with metal hydroxides, forming mixed gels. These structures exhibit very high water retention (>80 wt%) and extremely low permeability (Dobra et al., 2020; Hedwig et al., 2023).

Organic species, including residual extractants or degradation products, can stabilize colloids. They adsorb to particle surfaces, preventing aggregation and increasing cake resistance. Even at low concentrations (<100 mg/L), they can significantly alter filtration behavior (Han et al., 2024).

Other impurities, such as sulfate or chloride, influence hydrolysis equilibria and ionic strength. Their effect is indirect but can shift precipitation pathways and structural outcomes (Zhang et al., 2024).

Table 3 summarizes physicochemical factors affecting filterability, their effects, and typical ranges.

Table 3. Physicochemical factors controlling filterability in hydroxide precipitation, including typical ranges and their impact on structure and filtration performance. Adapted from Song et al. (2021), Deng et al. (2021), and Hedwig et al. (2023).

Factor	Typical range	Primary effect	Impact on filterability
pH	2–9	Controls hydrolysis	Defines precipitation regime
Supersaturation (S)	1–100	Controls nucleation/growth	High S → high α
Temperature	25–90 °C	Affects kinetics/viscosity	Higher T → better filtration
Ionic strength	0.01–1.0 M	Controls aggregation	Moderate I → improved k
Silica	0–500 mg/L	Gel formation	Strongly reduce spermeability
Organics	0–100 mg/L	Surface stabilization	Increases α

Table 3 shows that filterability is not controlled by a single variable. It emerges from the interaction between multiple physicochemical factors. In many cases, competing effects exist. For example, higher ionic strength promotes aggregation but may also increase solution viscosity.

The combined influence of these variables is illustrated in Figure 4, which shows how physicochemical parameters, including pH, supersaturation, temperature, and impurities, affect hydroxide structure and filterability.

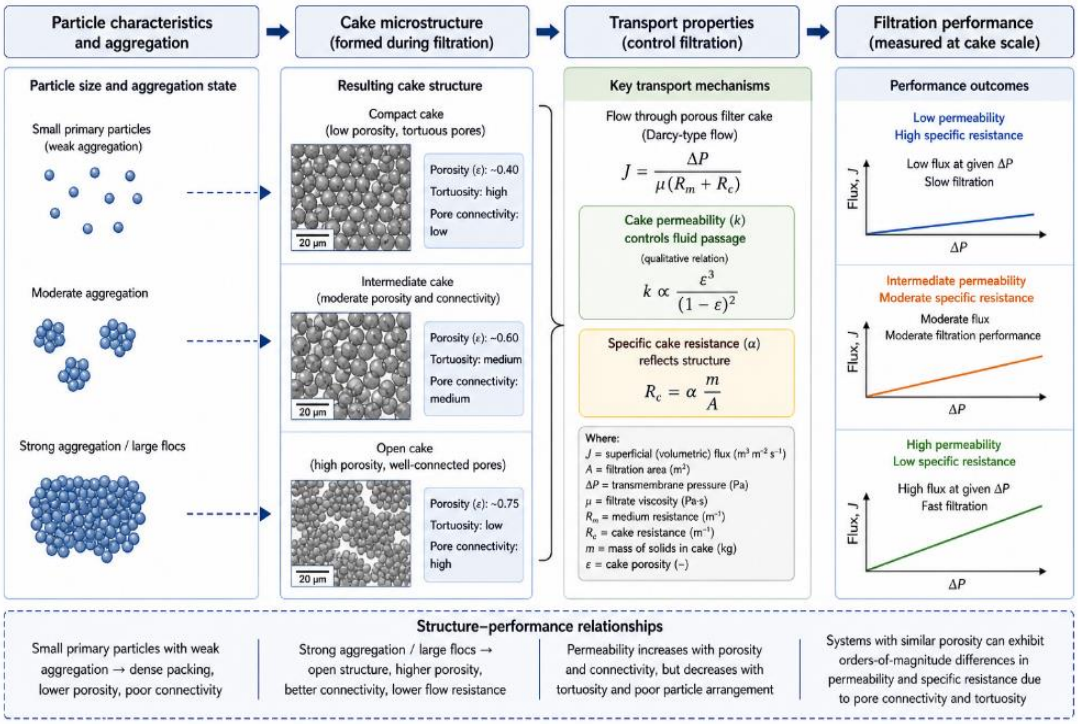

Figure 4. Influence of physicochemical parameters on hydroxide structure and filterability, showing transitions between dispersed particles, aggregates, and gel-like structures as a function of pH, supersaturation, temperature, and impurities. Adapted from Ibrahim et al. (2025) and Deng et al. (2021).

Figure 4 shows that filterability is governed by transitions between structural regimes. Dispersed particles, aggregates, and gels represent distinct states with markedly different permeability. These transitions are controlled by solution chemistry rather than by particle size alone.

The central insight is that filterability is highly sensitive to the chemical environment, not just the solid phase. This explains why similar precipitation systems can show markedly different filtration performance under slightly different operating conditions.

The next section examines how these physicochemical conditions translate into particle morphology and structure, and how these features control cake formation and permeability.

Morphology and Structure of Hydroxide Precipitates

The morphology and internal structure of hydroxide precipitates determine how particles pack, deform, and transmit fluid during filtration. These features are not fixed. They evolve from primary particle formation to aggregated networks and, in some systems, to partially densified solids. This section examines how crystallinity, aggregation, and aging define filtration behavior.

Amorphous vs Crystalline Structures

Hydroxide precipitates can form as amorphous, poorly ordered solids or as crystalline phases. This distinction is central to filtration performance. Amorphous hydroxides,

common in Fe^{3+} and Al^{3+} systems, have high water content and low structural rigidity. They form compressible cakes with specific resistance often exceeding 10^{12} m/kg (Romano et al., 2023).

In contrast, crystalline hydroxides or oxyhydroxides (e.g., goethite-like structures) exhibit more distinct particle boundaries. These solids pack into more permeable cakes, with α typically in the range of 10^{10}–10^{11} m/kg (Battaglia et al., 2024; Ventimiglia et al., 2025). The difference is not only in particle size but also in internal structure and surface roughness, both of which influence pore formation.

Crystallinity is controlled by temperature, residence time, and supersaturation. Operating at >60–80 °C with longer residence times favors crystallization. However, achieving this in industrial systems increases reactor volume and energy demand.

Aggregation and Fractal Structures

Primary particles rarely remain isolated. They aggregate into clusters that determine the final cake structure. These aggregates often exhibit fractal characteristics, with fractal dimensions typically ranging from 1.8 to 2.5, depending on the aggregation conditions (Sun et al., 2021; Zhao et al., 2022).

Aggregates with low fractal dimensions are open and porous, promoting fluid flow. Aggregates with high fractal dimensions are denser and less permeable. Aggregation is driven by interparticle forces, which are controlled by ionic strength, pH, and surface chemistry.

In hydroxide systems, aggregation is often more important than primary particle size. For example, 0.5-μm particles can form aggregates of 10–100 μm, significantly improving permeability if the structure remains open (Li et al., 2025; Zhang et al., 2024).

However, aggregation is not always beneficial. Excessive aggregation can produce compact clusters with low internal porosity. The key parameter is aggregate structure, not aggregate size. This distinction is often overlooked in experimental studies.

Aging and Structural Evolution

After formation, hydroxide precipitates undergo structural evolution, commonly referred to as aging. This evolution includes Ostwald ripening, densification, and partial crystallization. These processes occur over time scales ranging from tens of minutes to several hours (Wang et al., 2024; Wu et al., 2025).

During aging, smaller particles dissolve and redeposit onto larger ones, increasing the average particle size. Simultaneously, internal restructuring reduces water content and increases density. This can reduce specific cake resistance by an order of magnitude in some systems (Namayandeh et al., 2024).

However, industrial residence times are often insufficient for complete aging. As a result, many systems operate with metastable, partially structured solids. This explains the persistence of poor filterability even when precipitation conditions are optimized.

To connect morphology and filtration, Table 4. Morphological characteristics and their impact on filterability summarize key structural features and their effects.

Table 4. Morphological characteristics of hydroxide precipitates and their impact on filterability, including structural descriptors and typical filtration behavior. Adapted from Romano et al. (2023), Sun et al. (2021), and Wang et al. (2024).

Structuretype	Key feature	Typical scale	Filtration behavior
Amorphous gel	High water content (>80%)	<1 μm network	Very high α, low k
Crystalline particles	Defined structure	5–50 μm	Lower α, higher k
Loose aggregates	Low fractal dimension (~1.8–2.1)	10–100 μm	High permeability
Dense aggregates	High fractal dimension (~2.3–2.5)	10–50 μm	Moderate permeability
Aged structures	Densified particles	Variable	Reduced α

Table 4 shows that filterability depends on structural organization across multiple scales. Systems dominated by amorphous gels exhibit poor drainage, while aggregated or partially crystalline systems perform better. However, transitions between these states are continuous rather than discrete.

The evolution of morphology and structure is shown in Figure 5, illustrating how hydroxide precipitates evolve and affect filtration, linking primary particles, aggregates, and aged structures.

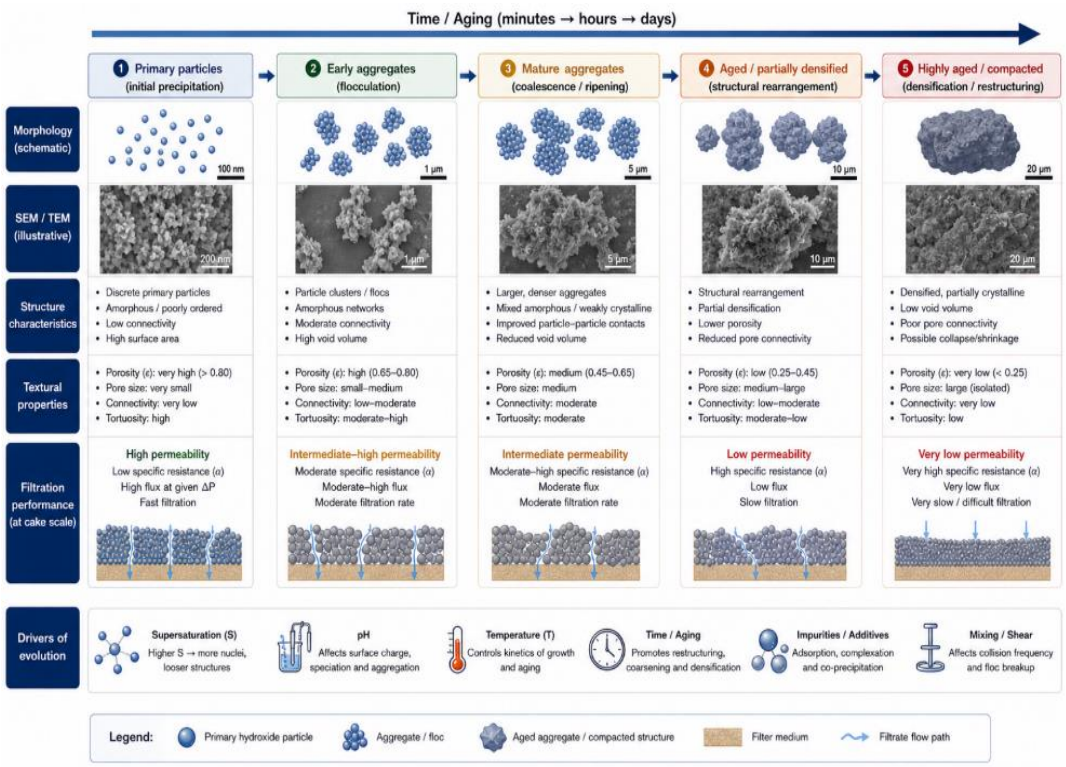

Figure 5. Structural evolution of hydroxide precipitates from primary particles to aggregates and aged structures, highlighting changes in porosity, connectivity, and filtration performance. Adapted from Zhao et al. (2022) and Wang et al. (2024).

Figure 5 highlights that filtration behavior is governed by structural evolution rather than initial particle size. The transition from amorphous networks to aggregated and partially densified structures defines permeability. Importantly, these transformations are controlled by process conditions and time, not only by chemistry.

A critical implication is that morphology must be engineered during precipitation, not corrected during filtration. This reinforces the need for integrated process design.

The next section examines process strategies to control these features and improve filterability.

Process Strategies to Improve Filterability

Improving filterability requires acting upstream, at the precipitation stage. Downstream corrections during filtration are limited. Process strategies must target supersaturation control, structural development, and aggregation pathways. Each strategy involves trade-offs between filtration performance, product purity, residence time, and cost.

Supersaturation Control

Supersaturation is the primary driver of particle formation. Reducing local supersaturation limits excessive nucleation and promotes growth. This can be achieved by slow base addition or staged neutralization (Fu et al., 2025; Lin et al., 2021).

In practice, multi-stage neutralization systems reduce supersaturation peaks by 30–70%, increasing particle size from <1 µm to 5–20 µm (Liao et al., 2024). This shift can reduce specific cake resistance by up to an order of magnitude.

However, staged systems require additional reactors and longer residence times. Industrial implementations typically increase residence time from 30 min to 60–120 min, thereby affecting CAPEX and footprint (Lu et al., 2025).

Seeded Precipitation

Seeded precipitation introduces pre-formed solids that serve as growth sites. This reduces nucleation and promotes crystal growth. Seed loading typically ranges from 1–10 wt% of solids (Zhao et al., 2024).

The effect is significant. Average particle size can increase by a factor of 2–5, while α decreases by 30–80%, depending on the system chemistry (Han et al., 2020). Seeded systems also improve reproducibility and reduce sensitivity to mixing.

Limitations include seed preparation, recycling, and potential contamination. In some systems, seeds may incorporate impurities, affecting product quality.

Dynamic pH Control

Dynamic pH control prevents overshoot and gel formation by gradually adjusting pH along the reactor instead of a fixed setpoint, avoiding the narrow ±0.5 pH zone where gelation typically occurs (Ibrahim et al., 2025).

Advanced control strategies include distributed dosing and feedback loops based on turbidity or conductivity. These approaches can stabilize precipitation and reduce variability. Reported reductions in α typically range from 20–50% (Ananda et al., 2023).

The main challenge is control complexity. Instrumentation and automation increase operational cost but improve consistency.

Elevated Temperature

Operating at elevated temperatures promotes crystallinity and reduces viscosity. Increasing the temperature from 25 °C to 80 °C can increase particle size by 2–5× and reduce viscosity by ~60% (Arampatzis et al., 2025; Tang et al., 2026).

This leads to improved filtration rates, often by a factor of 2–3, assuming a similar cake structure. Temperature also accelerates aging, thereby enhancing densification.

The drawback is energy consumption. Heating requirements typically add 5–15 USD per m³ of slurry, depending on the energy source and heat recovery. This limits applicability in low-margin operations.

Flocculation

Flocculation is widely used to improve apparent filterability. Polymers and coagulants promote aggregation, thereby increasing effective particle size. Typical dosages range from 10 to 200 g/t of solids (Guo et al., 2022; Jin et al., 2025).

Flocculation can reduce α by 50–90% and increase filtration flux by 2–5×. It is often the most cost-effective short-term option.

However, this improvement is often superficial. Flocs are mechanically weak and can collapse under pressure. More importantly, flocculants can trap impurities and increase moisture content, affecting downstream processing and product purity (Du et al., 2020).

→Critical point:

Flocculation improves filtration performance at the expense of structural control. It compensates for poor precipitation design rather than solving it.

Table 5. Process strategies for improving filterability and their quantitative impact summarizes the effects and trade-offs.

Table 5. Process strategies for improving filterability in hydroxide precipitation, including operational parameters, benefits, and limitations. Adapted from Fu et al. (2025), Zhao et al. (2024), and Guo et al. (2022).

Strategy	Key parameter	Typical improvement	Limitation
Supersaturation control	Staged neutralization	α ↓ 5–10×	Higher CAPEX
Seeded precipitation	1–10 wt% seeds	Particlesize ↑ 2–5×	Seed handling
Dynamic pH control	Controlled dosing	α ↓ 20–50%	Control complexity
Elevated temperature	60–90 °C	Flux ↑ 2–3×	Energy cost
Flocculation	10–200 g/t	α ↓ 50–90%	Purity loss

Table 5 shows no single universally optimal strategy; each targets different mechanisms. Combining strategies, like moderate supersaturation control with seeding, often yields better results than one alone.

The interaction among these strategies is shown in Figure 6. Integrated processes for controlling hydroxide structure and filterability link operating variables to structural outcomes.

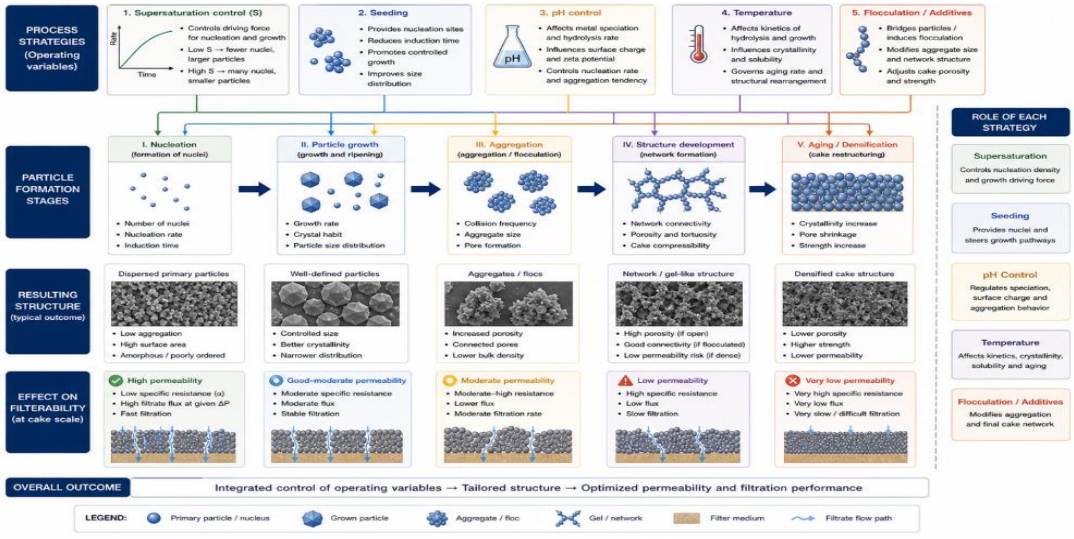

Figure 6. Integrated process strategies for controlling hydroxide structure and filterability, showing the influence of supersaturation, seeding, pH control, temperature, and flocculation on particle growth, aggregation, and final cake structure. Adapted from Lin et al. (2021) and Zhao et al. (2024).

Figure 6 highlights that process strategies act on different stages of particle formation. Supersaturation and pH control influence nucleation and growth. Seeding affects growth pathways. Temperature impacts crystallinity and aging. Flocculation modifies aggregation at the final stage.

The key insight is that filterability must be engineered during precipitation. Post-treatment strategies can improve performance but do not fundamentally alter the structure. This explains why many systems remain limited by filtration despite extensive downstream optimization.

The next section explores advanced approaches and emerging technologies that aim to overcome these limitations through improved process control and modeling.

Advanced Approaches and Emerging Technologies

Recent developments aim to control particle formation at its source. The focus is shifting from empirical tuning to engineered precipitation. These approaches target mixing, energy input, particle design, and predictive modeling. Their impact on filterability is promising but has not yet been fully translated to the industrial scale.

Advanced Reactors with Hydrodynamic Control

Reactor design strongly influences local supersaturation and mixing. Conventional stirred tanks generate broad mixing distributions. This leads to simultaneous nucleation and growth. Advanced reactors aim to reduce this heterogeneity.

Technologies include **static mixers, jet reactors, and microreactors**. These systems provide controlled mixing on short time scales (**milliseconds to seconds**). They reduce supersaturation peaks by up to **50–80%**, limiting excessive nucleation (Lu et al., 2025; Madlangbayan et al., 2025).

Jet reactors, for example, achieve high turbulence with Reynolds numbers above $\mathbf{10^4–10^5}$, promoting uniform conditions. Microreactors offer even tighter control but are limited in throughput. Scale-up remains a challenge due to fouling and residence time constraints (Bučinskaitė et al., 2026).

The main advantage is structural consistency. Narrower particle-size distributions and more uniform aggregates improve filtration. However, CAPEX is higher. Implementation requires redesigning existing circuits.

Ultrasound and Microwave-Assisted Precipitation

External energy fields influence nucleation and growth. Ultrasound induces cavitation, creating high-energy zones that enhance mixing and, depending on intensity, either promote nucleation or break aggregates (Arampatzis et al., 2025).

Typical ultrasound frequencies are 20–40 kHz with power densities of 10–100 W/L. At moderate levels, ultrasound enhances aggregation by increasing collision frequency. At high intensity, it fragments particles, producing more fines.

Microwave-assisted precipitation delivers rapid, uniform heating. This reduces temperature gradients and can accelerate crystallization. Heating rates can exceed 10–50 °C/min, significantly faster than in conventional systems (Jain et al., 2025).

Both techniques improve control over particle formation. However, their industrial application is limited by energy consumption and equipment complexity. Scale-up beyond pilot scale remains rare.

Particle Engineering

Particle engineering focuses on tailoring morphology to improve filtration. This includes controlling shape, size distribution, and internal structure.

Strategies include:

- Controlled aggregation using specific additives
- Surface modification to influence growth
- Directed crystallization under controlled conditions

Recent studies show fractal dimension control between 1.8 and 2.3, enabling permeability tuning (Wu et al., 2025; Zhou et al., 2024). Optimized structures can reduce α by up to ten times.

This approach is conceptually strong. It directly targets structure rather than relying on post-treatment. However, it requires precise control of process variables and often involves additional reagents.

Coupled Modeling (CFD + Precipitation + Filtration)

Modeling evolves from isolated descriptions to integrated frameworks that combine Computational Fluid Dynamics (CFD), population balance models (PBM), and filtration equations to predict particle formation and cake behavior (Raponi et al., 2025; Luo et al., 2025).

These models can simulate:

- Mixing and supersaturation fields
- Nucleation and growth kinetics
- Aggregation dynamics
- Filtration resistance evolution

Typical CFD simulations resolve millimeters to meters, while PBM tracks particles from nanometers to micrometers. This multiscale approach is necessary but computationally demanding.

Despite progress, validation remains limited, largely confined to laboratory data, with scarce industrial-scale validation, creating a gap between predictive capability and practical use (Para et al., 2022).

→Critical gap:

Modeling and industrial operation remain weakly connected. Predictive tools are not yet integrated into process design workflows.

To summarize these approaches, Table 6, Advanced technologies for improving filterability and their operational characteristics, compares their performance and limitations.

Table 6. Advanced approaches for improving filterability in hydroxide precipitation, including operating principles, typical ranges, and limitations. Adapted from Lu et al. (2025), Arampatzis et al. (2025), and Raponi et al. (2025).

Approach	Key parameter	Typical range	Benefit	Limitation
Advanced reactors	Mixing time	ms–s	Uniform supersaturation	Scale-upcomplexity
Ultrasound	Frequency	20–40 kHz	Enhanced aggregation control	High energy use
Microwave	Heating rate	10–50 °C/min	Faster crystallization	Limited scale
Particle engineering	Fractal dimension	1.8–2.3	Tuned permeability	Process complexity
Coupled modeling	Multiscale simulation	mm–m	Predictive design	Limited validation

Table 6 shows that advanced approaches provide better control over structure formation. However, they introduce complexity and cost. Their adoption depends on the balance between performance gains and economic constraints.

The integration of these technologies is shown in Figure 7, illustrating an advanced process framework for controlled hydroxide precipitation that connects reactor design, energy input, particle engineering, and modeling.

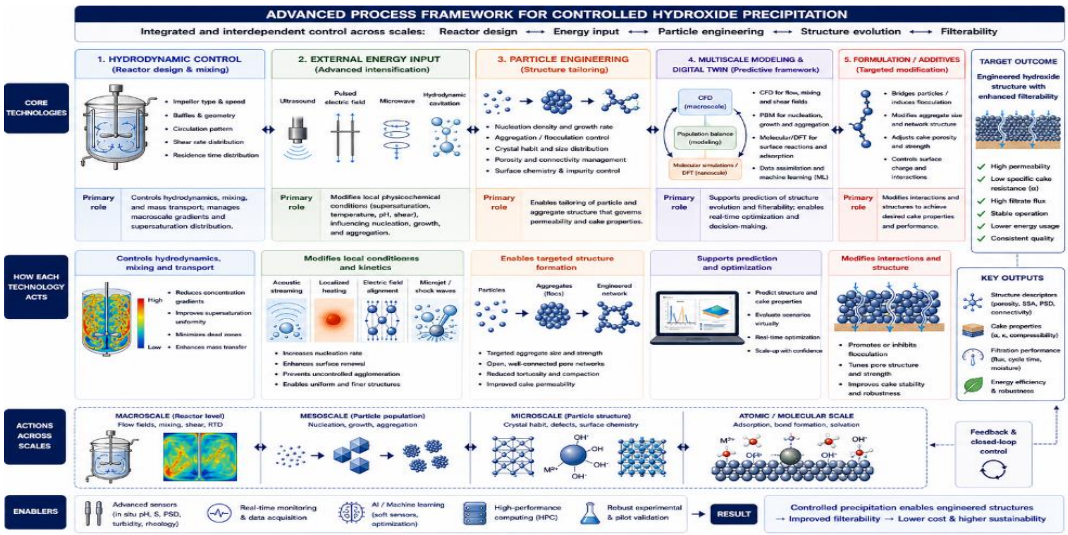

Figure 7. Advanced process framework for controlled hydroxide precipitation, integrating hydrodynamic control, external energy input, particle engineering, and multiscale modeling to improve filterability. Adapted from Luo et al. (2025) and Wu et al. (2025).

Figure 7 shows that advanced strategies act on multiple scales. Reactor design controls macroscopic mixing. Energy fields influence local nucleation. Particle engineering defines structure. Modeling links these effects into a predictive framework.

The key limitation is integration. Most approaches are applied in isolation. A unified strategy that combines reactor design, chemistry, and modeling is still missing in industrial practice.

The next section addresses the coupling between precipitation and solid–liquid separation, focusing on how upstream decisions define downstream filtration performance.

Coupling Between Precipitation and Solid–Liquid Separation

Precipitation and filtration are often treated as sequential unit operations. This representation is convenient but technically misleading. In hydroxide systems, the reactor not only removes metals from solution but also forms the solid structure that the filter must process. The filtration stage, therefore, inherits the consequences of pH control, supersaturation, mixing, aging, and aggregation (Audet et al., 2022; Jenssen et al., 2021).

The most important factor is cake structure. The precipitate formed in the reactor determines compressibility, permeability, and liquid retention. Fine amorphous hydroxides produce compressible cakes with high specific resistance. More crystalline or open-aggregated structures yield cakes with better drainage. In practical terms, a change in precipitation conditions can shift α from 10^{10} to $>10^{13}$ m/kg, which may require several times more filtration area to maintain the same throughput (Barros et al., 2025; Fan et al., 2026).

This coupling is summarized in Table 7. Links between precipitation conditions and filtration performance connect upstream process variables with downstream separation outcomes.

Table 7. Links between precipitation conditions and filtration performance in hydroxide systems. Adapted from Audet et al. (2022), Barros et al. (2025), and Fan et al. (2026).

Precipitation condition	Structural consequence	Filtration impact	Operational risk
High supersaturation	Fine primary particles	High α, low flux	Large filterarea
pH overshoot	Gel formation	Cake blinding	Rapid pressure rise
Poor mixing	Heterogeneous PSD	Unstable filtration	Variable cycle time
Insufficient aging	Hydrated amorphous solids	High cake moisture	Higher drying load
Controlled aggregation	Open pore network	Higher permeability	Better throughput
Excess flocculation	Weak flocs	Cake collapse under pressure	Poor reproducibility

Table 7 explains why filtration problems cannot be solved solely at the filter. Once a gel-like or highly compressible precipitate forms, increased pressure may worsen performance by collapsing pores. This is common in hydroxide cakes, where filtration flux may decline sharply as pressure rises from 1 to 5 bar. Higher pressure does not always mean higher productivity.

The coupling between precipitation and filtration is shown in Figure 8. It illustrates how reactor conditions influence cake structure and filtration in hydroxide systems.

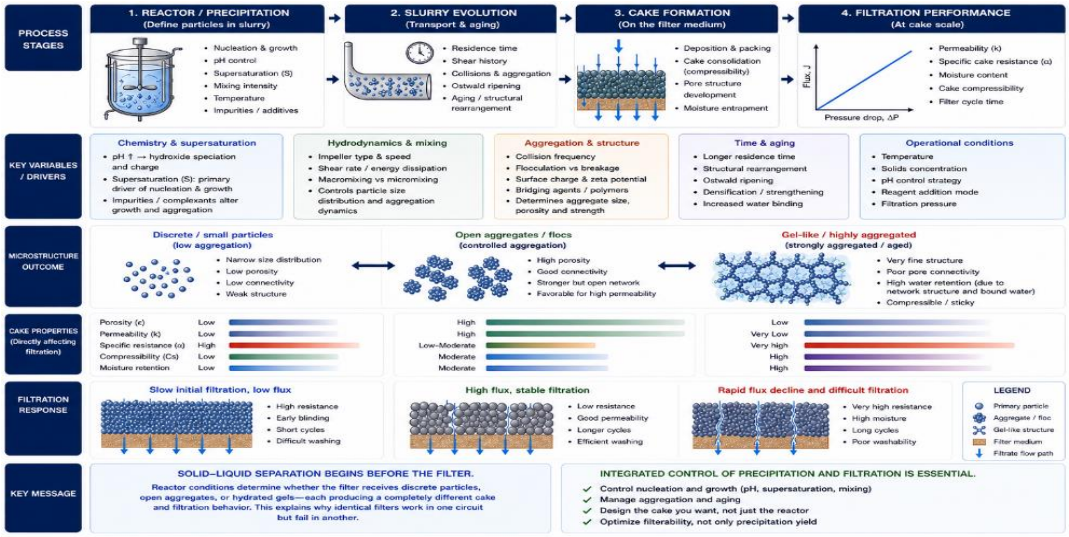

Figure 8. Integrated precipitation–filtration framework for hydroxide systems, showing how pH, supersaturation, mixing, aggregation, and aging define cake compressibility, permeability, and moisture retention. Adapted from Jenssen et al. (2021), Siddig et al. (2024), and Dittmer et al. (2025).

Figure 8 shows that solid–liquid separation starts before the slurry reaches the filter. The reactor controls whether the filter receives discrete particles, open aggregates, or hydrated gels, each of which affects filtration differently. This explains why identical filters work in one circuit but fail in another.

A key limitation in many hydrometallurgical flowsheets is the treatment of precipitation and filtration as separate steps. Precipitate removal efficiency is specified chemically, and filters are sized later by empirical tests. This weak workflow overlooks that slurry filterability is determined upstream.

A robust design should use coupled criteria to optimize precipitation not only for metal removal but also for cake resistance, permeability, compressibility, and moisture. Minimum data include pH profile, residence time, temperature, solids concentration, PSD, α, cake moisture, and pressure. Without these, scale-up is unreliable.

Precipitation and filtration are a coupled system; treating them separately causes oversized filters, instability, poor washing, and higher operational costs.

The next section examines industrial case studies where this coupling becomes evident in real hydrometallurgical circuits.

Industrial Case Studies

Industrial circuits support this review's main point: filtration performance is set during precipitation. Case studies in iron removal, aluminum, and rare earths show consistent patterns, often achieving chemical targets. However, filtration still limits progress (Hedwig et al., 2023; Chen et al., 2020).

Iron Removal (Jarosite and Goethite Systems)

Iron removal is vital in hydrometallurgy, mainly via jarosite precipitation at pH 1.5–2.5 and 90–100 °C, or goethite formation at pH 2.5–4.0 and similar temperatures (Chen et al., 2023; Choi et al., 2026).

Jarosite forms fine particles with poor filtration, typical α values are 10^{11}–10^{12} m/kg, and cake moisture exceeds 30–40 wt%. Goethite produces more crystalline particles, resulting in lower α (10^{10}–10^{11} m/kg) and better filtration.

However, these improvements come at a cost. Goethite processes require tighter pH control and longer residence times (2–6 h), which increase reactor volume and operating complexity. In many plants, the trade-off between precipitation efficiency and filtration performance remains unresolved (Oskouei et al., 2026).

Aluminum Hydroxide Precipitation

Aluminum precipitation, especially in sulfate systems or impurity removal, tends to form gels. At pH 4.5–6.5, $Al(OH)_3$ forms highly hydrated, amorphous solids that filter poorly.

Industrial data indicate filtration fluxes below 100 $L \cdot m^{-2} \cdot h^{-1}$ and cake moisture above 50 wt%, especially in systems with high supersaturation or poor mixing (Hedwig et al., 2023). The presence of silica further aggravates the problem by forming mixed gels.

Efforts to improve performance include seeding and temperature control. In some cases, particle size has increased from <1 µm to >10 µm, reducing α by 50–80%. However, achieving consistent control remains difficult due to sensitivity to process fluctuations (González et al., 2025).

Rare Earth Hydroxide Systems

Rare earth precipitation typically occurs at pH 6–8, often using NaOH or NH_4OH. These systems are widely used for separation and purification. The precipitates can be amorphous or partially crystalline, depending on the conditions.

Industrial observations show substantial variability in filtration behavior. In some cases, filtration rates exceed 300 $L \cdot m^{-2} \cdot h^{-1}$, while in others they fall below 100 $L \cdot m^{-2} \cdot h^{-1}$, even with similar PSD. This variability is linked to aggregation and aging effects rather than particle size alone (Lü et al., 2026; Cao et al., 2025).

Moisture content typically ranges from 20 to 45 wt%, depending on the structure. Systems with insufficient aging produce highly hydrated cakes. Longer residence times improve performance but reduce throughput.

To compare these industrial systems, Table 8, Summary of industrial hydroxide precipitation systems and filtration performance, consolidates key operating conditions and filtration metrics.

Table 8. Summary of industrial hydroxide precipitation systems and filtration performance, including operating conditions, cake resistance, and moisture content. Adapted from Chen et al. (2023), Hedwig et al. (2023), and Lü et al. (2026).

System	pH range	Temperature (°C)	α (m/kg)	Cake moisture (%)	Key issue
Jarosite	1.5–2.5	90–100	10^{11}–10^{12}	30–40	Fine particles
Goethite	2.5–4.0	80–100	10^{10}–10^{11}	25–35	Longer residence time
$Al(OH)_3$	4.5–6.5	25–80	10^{12}–10^{13}	40–60	Gel formation
$REE(OH)_3$	6–8	25–70	10^{10}–10^{12}	20–45	Structural variability

Table 8 highlights the wide variation in filtration performance across systems. Even within the same process, structural differences lead to large differences in α and moisture. This reinforces that chemical composition alone is insufficient to predict filterability.

Figure 9 shows the relationship between precipitation conditions and industrial filtration outcomes, combining typical operating windows and cake properties.

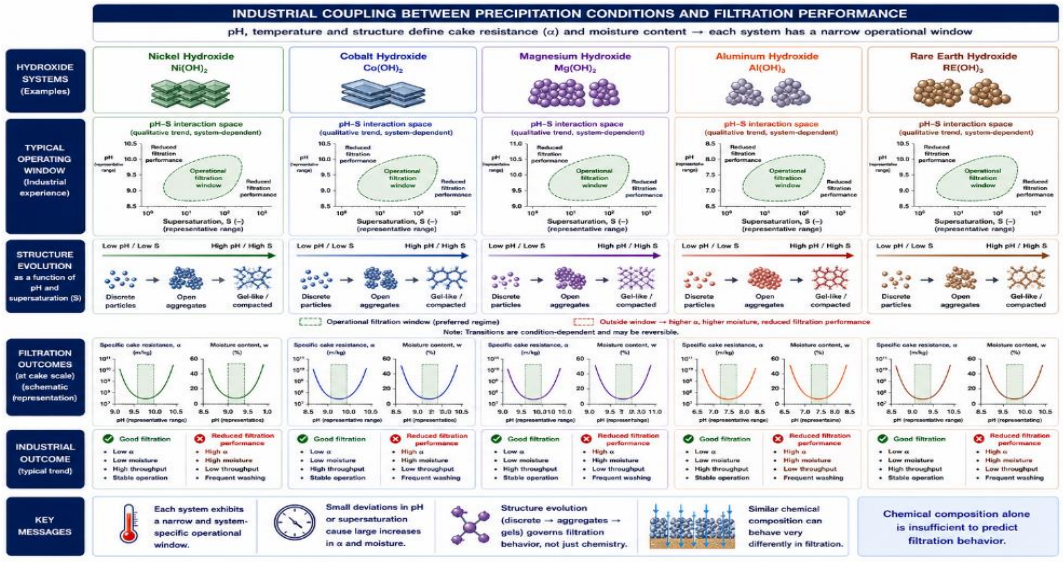

Figure 9. Industrial coupling between precipitation conditions and filtration performance, showing how pH, temperature, and structure influence cake resistance and moisture in different hydroxide systems. Adapted from Choi et al. (2026) and González et al. (2025).

Figure 9 shows that each system operates within a narrow window where filtration performance is acceptable. Outside this window, small deviations in pH or supersaturation can lead to large increases in α and moisture.

→Critical analysis:

Industrial studies rarely report key filtration parameters, such as specific cake resistance, permeability, or structural descriptors. Most publications focus on metal removal efficiency and chemical conditions, creating a gap between laboratory optimization and industrial performance.

Without quantitative filtration data, scale-up remains empirical. This explains why many plants require oversized filtration systems or operate below design capacity. The absence of integrated reporting prevents systematic improvement.

The next section identifies the main gaps in current research and outlines priorities for future work.

Critical Gaps and Research Needs

Current research on hydroxide precipitation remains fragmented. Most studies describe precipitation chemistry, whereas fewer link nucleation, structure, and filtration performance. This leaves a weak foundation for process scale-up. The central gap is not a lack of precipitation data but a lack of structure–filtration correlations (Deblonde et al., 2023; Davis & Demopoulos, 2023).

Missing Correlation Between Nucleation, Structure, and Filterability

Hydroxide formation reports include pH, metal removal, and particle size, but they don't explain differences in cake resistance among similar-sized precipitates. A better correlation also considers nucleation rate, aggregation, porosity, fractal dimension, compressibility, and cake moisture (Dobre et al., 2024).

The missing link is structural evolution. Nucleation generates primary particles. Aggregation defines pore networks. Aging changes density and water retention. Filtration then reflects the final structure. This sequence is rarely measured as a continuous process.

Lack of Experimental Standardization

Experimental methods are not standardized across studies. Different authors use different precipitation times, pH control strategies, mixing intensities, solids concentrations, and filtration pressures. This makes comparison difficult.

Minimum reporting should include pH profile, temperature, ionic strength, base addition rate, residence time, mixing intensity, solids concentration, PSD, cake moisture, specific cake resistance, and filtration pressure. Without these, reported filterability improvements are hard to reproduce (Xu et al., 2026).026).

Limited Industrial-Scale Data

Industrial data remains scarce. Many studies are conducted at the beaker or bench scale, often below 1–5 L. These systems do not replicate industrial mixing, residence time distribution, or slurry handling. Pilot-scale data above 100–1000 L are rarely reported.

This creates a scale-up problem. Small systems may show good precipitation efficiency but fail to predict filtration behavior. The lack of data on industrial cake resistance and permeability is a major limitation for process design (Ma et al., 2020; Estay et al., 2021).

Need for Coupled Precipitation–Filtration Tests

Future studies should evaluate precipitation and filtration as one coupled experiment. The precipitate should not be characterized only after formation. Instead, structural evolution should be monitored during pH adjustment, aging, aggregation, and filtration.

To consolidate these research needs, Table 9, Critical gaps and recommended research priorities for hydroxide filterability, summarizes the main limitations and proposed actions.

Table 9. Critical gaps and recommended research priorities for hydroxide filterability, including missing data, technical consequences, and proposed research actions. Adapted from Deblonde et al. (2023), Davis and Demopoulos (2023), and Dobre et al. (2024).

Critical gap	Current limitation	Technical consequence	Recommended priority
Nucleation–structure link	Final PSD reported without formation history	Poor prediction of α and k	Track supersaturation, nucleation, and aging
Structural metrics	Limited porosity and aggregate data	Weak structure–property correlations	Measure fractal dimension and pore connectivity
Filtration reporting	α, k, and compressibility often absent	Unreliable scale-up	Standardize cake resistance tests
Industrial validation	Few pilot or plant datasets	Over-reliance on bench data	Report data at >100–1000 L scale
Coupled testing	Precipitation and filtration tested separately	Misleading optimization	Use integrated precipitation–filtration protocols

Table 9 shows that the main research need is not only more data, but better-linked data. Precipitation variables must be reported together with structural and filtration metrics. This would allow comparison across systems and support predictive design.

The proposed research direction is summarized in Figure 10, which presents a research roadmap linking hydroxide formation, structure, and filterability, and connecting experimental design, structural characterization, and scale-up validation.

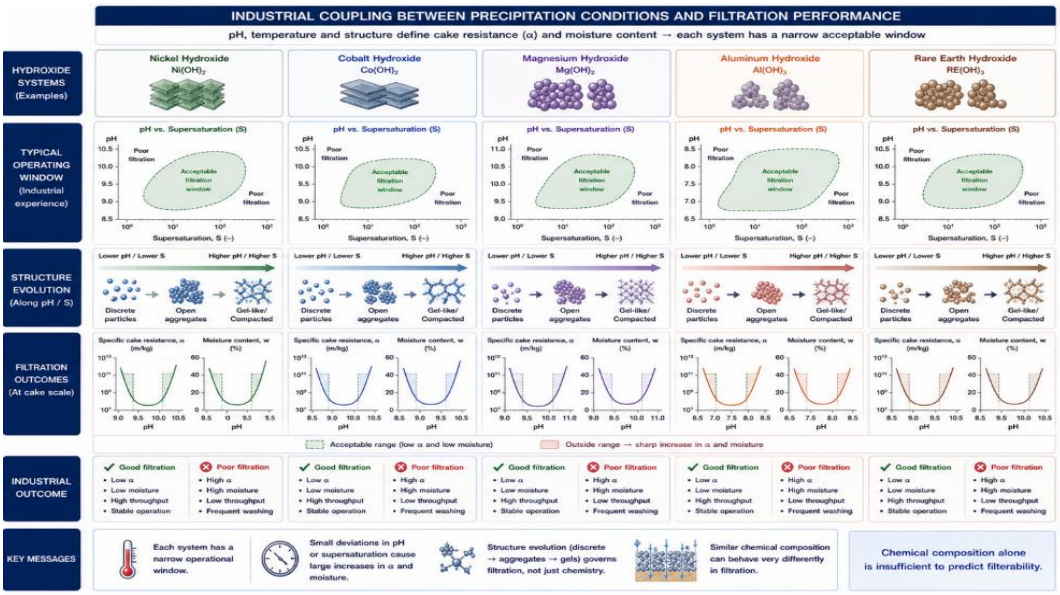

Figure 10. Research roadmap for linking hydroxide formation, structure, and filterability, showing the need for coupled precipitation–filtration experiments, structural descriptors, and industrial validation. Adapted from Xu et al. (2026), Ma et al. (2020), and Estay et al. (2021).

Figure 10 highlights a necessary shift in research strategy. Future work should move from isolated precipitation studies toward integrated datasets. These datasets must connect operating conditions, particle structure, cake behavior, and industrial performance.

The most urgent needs are clear: standardized filtration metrics, structural descriptors, and pilot-scale validation. Without these elements, hydroxide precipitation will remain optimized primarily for chemistry, while filtration will continue to limit plant performance.

Proposed Framework

The previous sections show a consistent pattern. Filtration performance is not an isolated outcome. It is the result of a sequence of coupled phenomena that begin at the molecular scale and propagate to plant operation. Current design approaches treat these steps separately. This section proposes an integrated framework that links precipitation conditions to filtration performance and process outcomes.

The framework is based on a causal chain:
Supersaturation → Nucleation/Growth → Particle Structure → Aggregation → Cake Structure → Filterability → Process Performance

Each step influences the next. Feedback loops also exist. For example, poor filterability increases residence time in downstream units, which can alter upstream operation. This interdependence is rarely captured in process design (Fu et al., 2025; Raponi et al., 2025).

To operationalize this concept, Table 10 summarizes the integrated framework linking precipitation variables to filtration, process performance, key variables, measurable outputs, and their impact on plant operation.

Table 10. Integrated framework linking precipitation variables to filtration and process performance, including key parameters, measurable outputs, and operational implications. Adapted from Lin et al. (2021), Raponi et al. (2025), and Luo et al. (2025).

Stage	Key variable	Measurable parameter	Typical range	Proces simpact
Supersaturation	S = C/C*	Supersaturation ratio	1–100	Controls nucleation
Nucleation/Growth	Rate balance	Particlesize (μm)	0.1–50	Defines primary particles
Particle structure	Morphology	Fractal dimension	1.8–2.5	Controls aggregation
Aggregation	Collision frequency	Aggregate size (μm)	10–100	Defines pore network
Cake structure	Packing	Porosity (ε)	0.6–0.9	Governs permeability
Filterability	Flow resistance	α (m/kg)	10^{10}–10^{13}	Defines filtration rate
Process performance	Throughput	Flux ($L \cdot m^{-2} \cdot h^{-1}$)	50–500	Determines CAPEX/OPEX

Table 10 shows that each stage has measurable parameters. These parameters can be monitored and controlled. However, in most industrial systems, only the first and last stages are measured. Intermediate variables such as aggregation and structure are rarely quantified. This limits predictive capability.

The full interdependence of these variables is illustrated in Figure 11, an integrated framework for hydroxide precipitation, structure evolution, and filterability, which represents the key conceptual contribution of this work.

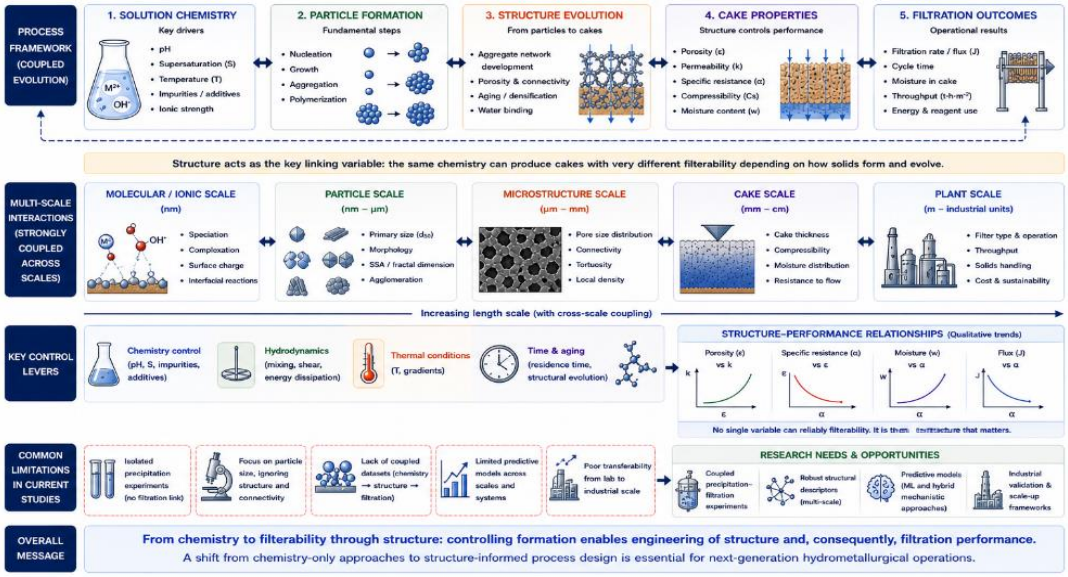

Figure 11. Integrated framework for hydroxide precipitation, structure evolution, and filterability, showing the sequential relationship between supersaturation, nucleation, aggregation, cake formation, and process performance, including feedback loops between filtration and upstream operation. Adapted from Fu et al. (2025), Luo et al. (2025), and Wu et al. (2025).

Figure 11 highlights two key points. First, filterability is not determined at the filtration stage. It is set earlier, during particle formation and aggregation. Second, the system includes feedback loops. For example, poor filtration increases cake thickness and cycle time, potentially requiring adjustments to upstream flow rates or reagent dosing.

From a design perspective, this framework suggests a shift from unit-operation optimization to system-level optimization. Rather than maximizing precipitation efficiency alone, processes should be designed to meet target values for α, permeability, and cake moisture. This requires integrating reaction engineering, particle design, and separation.

Quantitatively, reducing α from 10^{12} to 10^{11} m/kg can reduce the required filtration area by ~70–80%, depending on operating pressure. This directly translates into lower CAPEX and energy consumption. Such improvements cannot be achieved by filtration optimization alone. They require upstream control.

The framework also provides a basis for modeling. Each stage can be described using existing tools: thermodynamics for supersaturation, population balances for particle formation, and filtration models for cake behavior. The challenge is integration.

→Critical insight:

Process performance must be defined in terms of both chemical efficiency and separation efficiency. Treating these objectives independently leads to suboptimal design.

The next section presents the conclusions of this review and summarizes the main implications for research and industrial practice.

Conclusions

Hydroxide precipitation remains a central operation in hydrometallurgy, yet its performance is still assessed primarily by chemical metrics. This review shows that this approach is incomplete. Filtration, not precipitation, often determines process capacity. The key finding is that filterability is not an intrinsic property of hydroxide solids. It results from their formation history, structural evolution, and interaction with the liquid phase.

Across all systems analyzed, a consistent pattern emerges. Supersaturation, pH control, mixing, temperature, and impurities define nucleation and growth. These mechanisms determine particle structure, aggregation, and aging. The resulting cake structure governs permeability, compressibility, and moisture retention. Filtration performance is therefore a downstream expression of upstream conditions.

Industrial case studies confirm this coupling. Systems optimized for metal removal often show poor filtration performance. Specific cake resistance can vary by two to three orders of magnitude (10^{10}–10^{13} m/kg) within similar chemical systems. This variability leads to substantial differences in filtration area, energy consumption, and

operating costs. In practical terms, reducing cake resistance by one order of magnitude can cut filtration area requirements by 70–80%, yielding direct CAPEX and OPEX benefits.

Current design practices remain fragmented. Precipitation and filtration are treated as separate unit operations. Structural descriptors such as fractal dimension, pore connectivity, and compressibility are rarely measured. Industrial data often lack basic filtration parameters, including α, permeability, and cake moisture. This prevents reliable scale-up and limits process optimization.

Process strategies such as supersaturation control, seeding, temperature adjustment, and flocculation can improve filterability. However, their effectiveness depends on how they influence the formation of structure. Flocculation, in particular, often improves apparent filtration performance without addressing underlying structural limitations. This leads to unstable operation and potential losses in product quality.

Advanced approaches, including controlled hydrodynamic reactors, energy-assisted precipitation, particle engineering, and coupled modeling, offer new opportunities. These methods aim to control structure formation directly. However, their industrial implementation remains limited due to scale-up challenges and a lack of integration.

The framework proposed in this review provides a path forward. It links supersaturation, nucleation, aggregation, cake structure, and filtration performance into a single system. This approach enables the definition of design targets based on both chemical efficiency and separation performance.

Future work should focus on three priorities:

(i) **standardization of experimental methods**, including simultaneous measurement of precipitation and filtration parameters;
(ii) **quantification of structural descriptors**, such as fractal dimension, porosity, and compressibility;
(iii) **validation at pilot and industrial scale**, with datasets linking operating conditions to filtration performance.

Filtration performance should be engineered during precipitation, not corrected afterward. Combining reaction engineering with solid–liquid separation enhances efficiency, cuts costs, and supports scalable hydrometallurgical systems.

Funding

The author declares that no specific funding was received for this work.

Conflicts of Interest

The author declares no conflict of interest.

Availability of Data and Materials

The datasets generated and/or analyzed during the current study are available from the corresponding author on reasonable request.

Author Contributions

Conceptualization, methodology, analysis, and writing were performed by the author.

References

1. Abo Atia, T., Deferm, C., Machiels, L., Khoshkhoo, M., Riaño, S., & Binnemans, K. (2023). Solvent extraction process for refining cobalt and nickel from a “bulk hydroxide precipitate” obtained by bioleaching of sulfidic mine tailings. *Industrial & Engineering Chemistry Research, 62*(43), 17947–17958. https://doi.org/10.1021/acs.iecr.3c02612.
2. Amadghous, Y., Ait-Khouia, Y., Aboulaich, A., Zagriri, A., et al. (2025). Resource recovery from potash brine effluent: Integrated chemical precipitation and evaporative crystallization for zero liquid discharge and sustainable brine management. *Chemosphere*, *388*, 144700. https://doi.org/10.1016/j.chemosphere.2025.144700.
3. An, Y., Sato, Y., Wang, J., Guo, H., & Chen, G. (2023). Improving coprecipitation of chromium complexes with transition metals using self-floating carriers. *ACS ES & T Water*, *3*(12), 3952-3960..
4. An, Y., Sato, Y., Zheng, H., & Chen, G. (2023). Reusable self-floating carriers recover heavy metals from industrial wastewater through heterogeneous nucleation for resource reuse. *Journal of Hazardous Materials*, *447*, 130760. https://doi.org/10.1016/j.jhazmat.2023.130760.
5. Ananda, M. B., Vidathya, I.G.N.D., Ramadhani, M. *et al*. Effect of the pH with NaOH additives on the precipitation process of ferronickel leaching products from mini blast furnaces for $NiSO_4{\cdot}6H_2O$ synthesis. *Sādhanā* 49, 8 (2024). https://doi.org/10.1007/s12046-023-02377-9.
6. Antuñano, N., Balza de Vallejo, C., Rodriguez-Castaño, L., Zhang, Y., Galcerán, M., & Drewett, N. (2026). Particle engineering of recycled NMC precursors via integrated co-precipitation synthesis in the hydrometallurgical recycling of Li-ion batteries. *Powder Technology*, *479*, 122571. https://doi.org/10.1016/j.powtec.2026.122571
7. Arampatzis, A., Papaioannou, I., Van Gerven, T., & Stefanidis, G. D. (2025). Particle tuning in reactive crystallization via microwave-assisted temperature cycling for improved downstream performance. *Chemical Engineering and Processing - Process Intensification*, *211*, 110241. https://doi.org/10.1016/j.cep.2025.110241.
8. Arrisujaya, D., Yulizar, Y., & Saefumillah, A. (2025). Accelerated water purification with magnetite (Iron (II, III) Oxide) nanoparticles: Coagulation applications. *J. Chem. Rev*, *7*(1), 25-62.
9. Audet, D.R., Bach, M., Raahauge, B.E. (2022). Hydrate Precipitation, Classification and Filtration. In:

Raahauge, B.E., Williams, F.S. (eds) Smelter Grade Alumina from Bauxite. Springer Series in Materials Science, vol 320. Springer, Cham. https://doi.org/10.1007/978-3-030-88586-1_7.

10. Balinski, A., Wiche, O., Kelly, N., Reuter, M. A., & Scharf, C. (2020). Separation of rare earth elements from contaminants and valuable components by in-situ precipitation during the hydrometallurgical processing of eudialyte concentrate. *Hydrometallurgy, 194*, 105345. https://doi.org/10.1016/j.hydromet.2020.105345
11. Bao, S., Wang, Z., Ding, W., Zhang, Y., Liu, C., Zhang, H., Chen, B., Xin, C., & Xue, K. (2026). Emerging green recycling technologies for spent lithium-ion batteries: A comprehensive review integrating and innovating traditional methods. *Green Chemistry, 28*, 3394–3431. https://doi.org/10.1039/D5GC05709D.
12. Barros, L., Piaggio, G., Quilaqueo, M., Seriche, G., Pérez, K., Barraza, B., Romero, J., Ruby-Figueroa, R., & Estay, H. (2025). Analysis of membrane fouling during microfiltration of copper sulfide precipitates. *Separation and Purification Technology, 354*(Part 5), 129165. https://doi.org/10.1016/j.seppur.2024.129165.
13. Battaglia, G., Ventimiglia, L., Vicari, F., Tamburini, A., Cipollina, A., & Micale, G. (2024). Characterization of $Mg(OH)_2$ powders produced from real saltworks bitterns at a pilot scale. *Powder Technology, 443*, 119918. https://doi.org/10.1016/j.powtec.2024.119918.
14. Binnemans, K., Jones, P. T., Manjón Fernández, Á., & Masaguer Torres, V. (2020). Hydrometallurgical processes for the recovery of metals from steel industry by-products: A critical review. *Journal of Sustainable Metallurgy, 6*(4), 505–540. https://doi.org/10.1007/s40831-020-00306-2.
15. Bučinskaitė, P., Ha, T.-H., Urniezaite, I., & Lu, M.-C. (2026). Homogeneous crystallization of nickel contaminated industrial wastewater using fluidized bed technology. *Separation and Purification Technology, 395*(Part 1), 137705. https://doi.org/10.1016/j.seppur.2026.137705.
16. Cao, Z., Zhao, D., Ma, B. *et al*. The Precipitation Performance of Regeneration Magnesium Oxide in the Separation of Valuable Components in Laterite Solution. *J. Sustain. Metall.* 11, 4502–4512 (2025). https://doi.org/10.1007/s40831-025-01268-z.
17. Chen, J., Qiu, J., Chen, X., Peng, B., Qiu, Y., & Xiao, Y. (2023). The precipitation process for a rare earth leach solution with calcium oxide in the presence of ascorbate and calcination to oxide of high purity. *Hydrometallurgy, 221*, 106111. https://doi.org/10.1016/j.hydromet.2023.106111.
18. Chen, S., Huang, X., Feng, Z., Xu, Y., Wang, M., Xia, C., & Zhao, L. (2020). Behavior of rare earth, iron, and phosphorus during purification of rare earth sulfate leach solution using magnesium oxide. *Hydrometallurgy, 196*, 105377. https://doi.org/10.1016/j.hydromet.2020.105377.
19. Chernyaev, A., Wilson, B. P., & Lundström, M. (2021). Study on valuable metal incorporation in the Fe–Al precipitate during neutralization of LIB leach solution. *Scientific Reports, 11*, 23283. https://doi.org/10.1038/s41598-021-02019-2.
20. Chernyaev, A., Zhang, J., Seisko, S., Louhi-Kultanen, M., & Lundström, M. (2023). Fe and Al removal by phosphate and hydroxide precipitation from synthetic NMC Li-ion battery leach solution. *Scientific Reports, **13***, 48247. https://doi.org/10.1038/s41598-023-48247-6
21. Choi, K. H., Jang, J., Bedrossian, S., & Azimi, G. (2026). Impurity control and post-crystallization purification of $CoSO_4 \cdot 7H_2O$ for battery-grade cobalt production. *Hydrometallurgy, 241*, 106661. https://doi.org/10.1016/j.hydromet.2026.106661.
22. Choi, Y., Mun, S., & Lee, K. B. (2025). Direct synthesis of vertically oriented Co–Mg–Al layered double hydroxide on spherical γ-Al_2O_3 for passive NOx adsorber. *Applied Surface Science, 687*, 162248. https://doi.org/10.1016/j.apsusc.2024.162248.
23. Comel, J., Meux, E., Leclerc, N., & Diliberto, S. (2021). Use of phytic acid for selective precipitation of undesirable metals (Al, Fe, Pb) contained in the leachates from hydrometallurgical processes. *Journal of Environmental Chemical Engineering, 9*(4), 105450. https://doi.org/10.1016/j.jece.2021.105450.
24. Davis, K., & Demopoulos, G. P. (2023). Hydrometallurgical recycling technologies for NMC Li-ion battery cathodes: Current industrial practice and new R & D trends. *RSC Sustainability, 1*(8), 1932–1951. https://doi.org/10.1039/D3SU00142C.
25. Deblonde, G. J.-P., Chagnes, A., & Côté, G. (2022). Recent advances in the chemistry of hydrometallurgical methods. *Separation and Purification Reviews, 52*(20). https://doi.org/10.1080/15422119.2022.2088389
26. Deng, N., Li, Z., Hu, Y., et al. (2021). Coprecipitation of Fe/Cr hydroxides with organics: Roles of organic properties in composition and stability of the coprecipitates. *Environmental Science & Technology*. https://doi.org/10.1021/acs.est.0c04712.
27. Deng, Z., Oraby, E. A., & Eksteen, J. J. (2020). Sulfide precipitation of copper from alkaline glycine–cyanide solutions: Precipitate characterisation. *Minerals Engineering, 145*, 106102. https://doi.org/10.1016/j.mineng.2019.106102
28. Dias, M. E. d. M. G., Tenório, J. A. S., Espinosa, D.C.R. *et al*. Recycling of Li-Ion Batteries: Recovery of Critical Metals by Hydrometallurgy. *JOM* 78, 1188–1199 (2026). https://doi.org/10.1007/s11837-025-07677-5.

29. Dighe, P. S., Redekar, R. S., Tarwal, N. L., & Sarawade, P. B. (2025). Unveiling the performance of nickel cobalt-layered double hydroxide/reduced graphene oxide composite for high performance aqueous supercapacitor. *Journal of Power Sources, 634*, 236474. https://doi.org/10.1016/j.jpowsour.2025.236474
30. Dittmer, D., Andary, M., Diaz, F., & Friedrich, B. (2025). Evaluation of filter cake washing processes in hydrometallurgical battery recycling of lithium-ion batteries to optimize recoveries. *Metals, 15*(11), 1262. https://doi.org/10.3390/met15111262
31. Djoudi, N., Le Page Mostefa, M., &Muhr, H. (2021). Hydrometallurgical process to recover cobalt from spent Li-ion batteries. *Resources, 10*(6), 58. https://doi.org/10.3390/resources10060058.
32. Dong, Y., Zhang, M., & Xie, C. (2020). Effect of reaction conditions on agglomeration of aluminum hydroxide in the recovery of waste aluminum-catalyst. *Separation and Purification Technology, 248*, 116978. https://doi.org/10.1016/j.seppur.2020.116978.
33. Dong, Z., Mattocks, J. A., Deblonde, G. J.-P., Hu, D., Jiao, Y., Cotruvo, J. A., & Park, D. M. (2021). Bridging hydrometallurgy and biochemistry: A protein-based process for recovery and separation of rare earth elements. *ACS Central Science, 7*(11), 1798–1808. https://doi.org/10.1021/acscentsci.1c00724.
34. Dobre, T., Isopencu, G. O., Ahmed, S. B., & Deleanu, I. M. (2024). Heavy metal pollution and solutions for its control: General aspects with a focus on cobalt removal and recovery from aqueous systems. *Chem Engineering, 8*(6), 118. https://doi.org/10.3390/chemengineering8060118
35. Du, C.-m., Gao, X., Ueda, S., & Kitamura, S.-y. (2022). Recovery of high-quality phosphate from steelmaking slag by a hydrometallurgical process. *Science of The Total Environment, 819*, 153125. https://doi.org/10.1016/j.scitotenv.2022.153125.
36. Du, X., Yang, W., Liu, Y., Zhang, W., Wang, Z., Nie, J., Li, G., & Liang, H. (2020). Removal of manganese, ferrous and antibiotics from groundwater simultaneously using peroxymonosulfate-assisted in-situ oxidation/coagulation integrated with ceramic membrane process. *Separation and Purification Technology, 252*, 117492. https://doi.org/10.1016/j.seppur.2020.117492
37. Emil-Kaya, E., Kaya, O., Stopic, S., Gürmen, S., & Friedrich, B. (2023). Recycling of NdFeB magnets: Model supported iron minimization via in-situ hydrolysis during leaching and hematite precipitation in an autoclave. *Hydrometallurgy, 222*, 106192. https://doi.org/10.1016/j.hydromet.2023.106192.
38. Estay, H., Barros, L., & Troncoso, E. (2021). Metal sulfide precipitation: Recent breakthroughs and future outlooks. *Minerals, 11*(12), 1385. https://doi.org/10.3390/min11121385
39. Fan, Y., Wen, P., Ma, X., Dong, X., Chen, R., Yang, M., Xiao, W., & Mu, Y. (2026). Enhancement of ultra-high-pressure dewatering of fine coal slurry: Synergistic regulation mechanism of pore interface chemistry by polycarboxylate-CaO. *Fuel, 412*, 138136. https://doi.org/10.1016/j.fuel.2025.138136.
40. Faris, N., White, J., Magazowski, F., Fischmann, A., Jones, L. A., Tardio, J., Madapusi, S., Grocott, S., & Bhargava, S. K. (2021). An investigation into potential pathways for nickel and cobalt loss during impurity removal from synthetic nickel laterite pressure acid leach solutions via partial neutralisation. *Hydrometallurgy, 202*, 105595. https://doi.org/10.1016/j.hydromet.2021.105595
41. Fu, Z., Wang, Y., Shi, X., Zhou, D., Li, Z., Jin, P., Li, K., Zhang, G., Mei, A., Sun, B., & Zhang, Y. (2025). Supersaturation mechanisms and regulation strategies in nucleation-induced crystallization for high-purity fluoride recovery from photovoltaic wastewater. *Chemical Engineering Journal, 523*, 168353..
42. Gafiullina, A., Mamelkina, M., Vehmaanperä, P., Kinnarinen, T., & Häkkinen, A. (2020). Pressure filtration properties of sludge generated in the electrochemical treatment of mining waters. *Water Research, 181*, 115922. https://doi.org/10.1016/j.watres.2020.115922.
43. Gong, J., Wang, J., Zhu, J., Jin, Y., & Li, J. (2026). Recovery of phosphorus from rare earth leachate and preparation of battery-grade iron phosphate. *Separation and Purification Technology, 395*(Part 1), 137687. https://doi.org/10.1016/j.seppur.2026.137687
44. González, C., Quilaqueo, M., Piaggio, G., Barros, L., Quintero, Y. M., García, A., & Estay, H. (2025). Membrane distillation–crystallization of lithium hydroxide. *Sustainable Materials and Technologies, 45*, e01457. https://doi.org/10.1016/j.susmat.2025.e01457.
45. Guo, J., Zhou, Z., Sun, D., Zeng, L., Ming, Q., Xing, Y., Huang, Z., & Zhao, X. (2022). Recovering double-metal hydroxides precipitate from desalination process of saline wastewater as conditioner for excess sludge dewatering. *Chemical Engineering Journal, 434*, 134787. https://doi.org/10.1016/j.cej.2022.134787.
46. Han, H., Sun, W., Sun, W., & Hu, Y. (2020). Magnetic separation of impurities from hydrometallurgy solutions and waste water using magnetic iron ore seeding. In V. Shatokha (Ed.), *Iron Ores*. Intech Open. https://doi.org/10.5772/intechopen.93728
47. Han, R., Gao, Y., Jia, Y., & Wang, S. (2024). Heterogeneous precipitation behavior and mechanism during the adsorption of cationic heavy metals by biochar: Roles of inorganic components. *Journal of*

Hazardous Materials, 480, 136322. https://doi.org/10.1016/j.jhazmat.2024.136322.

48. Hedwig, S., Yagmurlu, B., Peters, E. M., Misev, V., Hengevoss, D., Dittrich, C., Forsberg, K., Constable, E. C., & Lenz, M. (2023). From trace to pure: Pilot-scale scandium recovery from TiO_2 acid waste. *ACS Sustainable Chemistry & Engineering, 11*(15), 5883–5894.
49. He, Y., Wang, K., Zhao, Y., Chen, Z., & Han, H. (2024). Urease-producing bacteria enhance the adsorption of Cd on organo-Fe hydroxide coprecipitates. *Separation and Purification Technology*, *344*, 127266. https://doi.org/10.1016/j.seppur.2024.127266.
50. Huang, F., Rong, S., Tao, S., Chu, H., & Zhang, C. (2024). A novel chitosan/biochar-modified eco-concrete with balanced mechanical, planting, and water purification performance for riparian restoration. *Journal of Cleaner Production, 481*, 144144. https://doi.org/10.1016/j.jclepro.2024.144144.
51. Hu, Y. (2025). Supersaturation-controlled morphology and phase evolution of NiCo LDH in controllable and continuous flow synthesis. *PLOS ONE*. https://doi.org/10.1371/journal.pone.0335668.
52. Ibrahim, M. H., Batstone, D., Vaughan, J., & Steel, K. (2025). CO_2-induced pH control reduces cathode scaling and enhances electrochemical acid recovery from nickel laterite waste solution. *Separation and Purification Technology, 379*, 135075. https://doi.org/10.1016/j.seppur.2025.135075.
53. Jenssen, I. B., Ucar, S., Dotterud, O. M., Bøckman, O., & Andreassen, J.-P. (2021). Investigating the effects of process parameters on the filtration performance of ferric hydroxide in a continuous MSMPR reactor. *Hydrometallurgy, 202*, 105594. https://doi.org/10.1016/j.hydromet.2021.105594
54. Jin, X., Shang, Y., Qian, Z., Xu, L., Liu, M., Hu, S., Wang, Y., Xu, L., Bai, X., Shi, X., Jin, P., & Wang, X. C. (2025). Prolonged stirring pelleting coagulation for the enhanced treatment of fresh leachate: Removal performance and floc characteristics. *Separation and Purification Technology, 353*(Part A), 128365. https://doi.org/10.1016/j.seppur.2024.128365.
55. Kalaitzidou, K., Chioti, E., Asimakidou, T., Karfaridis, D., Vourlias, G., Mitrakas, M., & Simeonidis, K. (2022). Tuning the Fe(II)/hydroxide ratio during synthesis of magnetite nanoparticles to maximize Cr(VI) uptake capacity. *Water, 14*(9), 1335. https://doi.org/10.3390/w14091335.
56. Laskar, C., & Binnemans, K. (2026). Recovery of metallic iron from the loaded organic phase after solvent extraction by precipitation–stripping with hydrogen gas. *RSC Advances, 16*, 12374–12382. https://doi.org/10.1039/D6RA00829A.
57. Lemmens, L., Vanwezer, X., Raiguel, S., Lommelen, R., Forsberg, K., Van Gerven, T., & Binnemans, K. (2026). Solubility and antisolvent crystallization of lithium hydroxide monohydrate in various organic solvents. *Physical Chemistry Chemical Physics, 28*, 6743–6755. https://doi.org/10.1039/D5CP04491J.
58. Li, H., Gan, S., Yue, C., Yan, Q., Xue, J., & Zhang, Y. (2025). Superhydrophilic membrane coupled with hydroxide ion-assisted bubbles for efficient separation of surfactant-stabilized oil/water emulsions. *Journal of Hazardous Materials, 472*, 134547.https://doi.org/10.1016/j.jhazmat.2024.134547.
59. Li, Z., Zhao, M., Tian, R., Shi, W., Tian, Y., Bai, Y., & Xu, M. (2024). A coupling strategy to produce highly dispersed ultrathin antioxidant intercalated layered double hydroxides for enhancing performance of polypropylene composites. *Chemical Engineering Journal, 476*, 146451.https://doi.org/10.1016/j.cej.2023.146451
60. Liao, P.-L., Effendi, L. W., Mahasti, N. N. N., Chang, K.-Y., & Huang, Y.-H. (2024). Homogeneous crystallization of nickel as Ni_3S_4 in a fluidized bed reactor with supersaturation control. *Journal of Environmental Chemical Engineering, 12*(6), 114596. https://doi.org/10.1016/j.jece.2024.114596.
61. Lin, J.-Y., Mahasti, N. N. N., & Huang, Y.-H. (2021). Fluidized-bed crystallization of barium perborate for continuous boron removal from concentrated solution: Supersaturation as a master variable. *Separation and Purification Technology, 278*, 119588. https://doi.org/10.1016/j.seppur.2021.119588.
62. Liu, S., Li, Y., Guo, H., Liu, X., & Cao, J. (2025). Preparation of nano-hexagonal flake magnesium hydroxide from seawater brine and the crystallization-based separation of inorganic salt products from the mother liquor. *Desalination, 612*, 118954. https://doi.org/10.1016/j.desal.2025.118954.
63. Liu, X., Zhi, Y., Yuan, Y., Zhong, H., Chen, Y., Shi, G., & Yang, M. (2025). Phosphorus removal by concrete-based layered double hydroxides: The influence of titration mode for continuous flow coprecipitation. *Applied Clay Science, 265*, 107682. https://doi.org/10.1016/j.clay.2024.107682.
64. Lu, T.-K., Lin, T.-Y., Huang, C.-P., Liao, P.-L., Chang, K.-Y., & Huang, Y.-H. (2025). Optimized fluidized bed homogeneous crystallization process for recovering magnesium as granulated magnesium hydroxide from high-salinity water. *Separation and Purification Technology, 377*(Part 3), 134407. https://doi.org/10.1016/j.seppur.2025.134407.
65. Lü, H., Huang, Z., Wang, X., Tian, F., Lu, X., Peng, X., & Hu, X. (2026). Near closed-loop recycling of strongly acidic wastewater via selective fluoride and heavy metal removal. *Journal of Water Process Engineering, 81*, 109375. https://doi.org/10.1016/j.jwpe.2025.109375.
66. Luo, P., Zhang, Y., Shen, Z., Hu, Y., Chen, H., & Ma, Z.-F. (2026). Physics-informed machine learning

framework for predictive control of particle size distribution in $Ni_{1/3}Fe_{1/3}Mn_{1/3}(OH)_2$ synthesis. *Chemical Engineering Science, 320*(Part B), 122600. https://doi.org/10.1016/j.ces.2025.122600

67. Ma, P., Hou, Y., Chen, Z., Su, L., Li, L., Liu, N., & Zhang, Z. (2021). Enhanced stability of $CsPbBr_3$ quantum dots by anchoring on hierarchical three-dimensional layered double hydroxide. *Chemical Engineering Journal*, 405, 126966. https://doi.org/10.1016/j.cej.2020.126966
68. Ma, Y., Svärd, M., Xiao, X., Gardner, J. M., Olsson, R. T., & Forsberg, K. (2020). Precipitation and crystallization used in the production of metal salts for Li-ion battery materials: A review. *Metals, 10*(12), 1609. https://doi.org/10.3390/met10121609.
69. Madlangbayan, G. A. C., Quiton, K. G. N., Ha, T.-H., & Lu, M.-C. (2025). Enhanced recovery of lead and nitrate via fluidized-bed reactor: Recovery of insoluble salts from simulated gold cyanidation effluent. *Chemical Engineering Journal, 524*, 169101. https://doi.org/10.1016/j.cej.2025.169101
70. Mandarawala, M.A., Mahajan, A.N., Koradia, S.K. *et al*. Precipitation Inhibitor–Stabilized Supersaturated SNEDDS of Ticagrelor: Design, Optimization, and Pharmacokinetic Study. *BioNanoSci*. 15, 513 (2025). https://doi.org/10.1007/s12668-025-02135-7.
71. Mhaske, V. P., & Yadav, M. D. (2024). Synthesis and characterization of coprecipitated layered NCM oxide as cathode for sodium-ion batteries: Kinetics and hydrodynamics studies. *Chemical Engineering Science***,** *295*, 120177. https://doi.org/10.1016/j.ces.2024.120177
72. Miciletta, F., Battaglia, G., Scelfo, G., Vassallo, F., Vicari, F., Tamburini, A., Cipollina, A., & Micale, G. (2025). A novel pilot-scale crystallizer for the production of $Mg(OH)_2$ powders from saltworks bitterns. *Chemical Engineering Transactions, 119*, 7–12. https://doi.org/10.3303/CET25119002.
73. Nadagouda, M. N., Varshney, G., Varshney, V., & Hejase, C. A. (2024). Recent advances in technologies for phosphate removal and recovery: A review. *ACS Environmental Au*, *4*(6), 271–291. https://doi.org/10.1021/acsenvironau.3c00069.
74. Namayandeh, A., Borkiewicz, O. J., Sassi, M., Rosso, K. M., & Michel, F. M. (2024). Formation and transformation of iron oxy-hydroxide precursor clusters to ferrihydrite. *Environmental Science: Nano***,** ***11***, 3966–3978. https://doi.org/10.1039/D3EN00930K
75. Ning, D., Lu, Z., Tian, C., Yan, N., & Hua, L. (2024). Hierarchical and superwettable cellulose acetate nanofibrous membranes decorated via 3D flower-like layered double hydroxides for efficient oil/water separation. *Separation and Purification Technology, 342*, 127052. https://doi.org/10.1016/j.seppur.2024.127052.
76. Oskouei, A. E., Asgharzadeh, H., Shekaari, H., & Golmohammadi, B. (2026). Industrial extraction of lithium from Urmia Lake using precipitation and evaporation methods. *Scientific Reports, 16*, 9893. https://doi.org/10.1038/s41598-026-09893-0.
77. Page, M. J., Moher, D., Bossuyt, P. M., Boutron, I., Hoffmann, T. C., Mulrow, C. D., Shamseer, L., Tetzlaff, J. M., Akl, E. A., Brennan, S. E., Chou, R., Glanville, J., Grimshaw, J. M., Hróbjartsson, A., Lalu, M. M., Li, T., Loder, E. W., Mayo-Wilson, E., McDonald, S., McGuinness, L. A., Stewart, L. A., Thomas, J., Tricco, A. C., Welch, V. A., Whiting, P., & McKenzie, J. E. (2021). PRISMA 2020 explanation and elaboration: Updated guidance and exemplars for reporting systematic reviews. *BMJ, 372*, n160. https://doi.org/10.1136/bmj.n160.
78. Para, M. L., Alidoost, M., Shiea, M., Boccardo, G., Buffo, A., Barresi, A. A., & Marchisio, D. (2022). A modelling and experimental study on the co-precipitation of $Ni_{0.8}Mn_{0.1}Co_{0.1}(OH)_2$ as precursor for battery cathodes. *Chemical Engineering Science, 254*, 117634. https://doi.org/10.1016/j.ces.2022.117634.
79. Petersen, J., & van Staden, P. (2025). Heap leaching: Process, principles, and practical considerations. In S. Seetharaman (Ed.), *Treatise on Process Metallurgy* (Vol. 2B, pp. 333–345). Elsevier. https://doi.org/10.1016/B978-0-443-40294-4.00029-3.
80. Prajapati, D. K., Bardhan, A., & Sharma, S. (2025).Microwave-assisted synthesis of zinc oxide nanoflowers for improving the rheological and filtration performance of high-temperature water-based drilling fluids. *Journal of Dispersion Science and Technology*. Advance online publication. https://doi.org/10.1080/01932691.2024.2362105.
81. Qi, F., Cao, J., Zhu, G., Sun, J., Li, S., Wu, W., Zheng, J., Li, H., & Zhang, Y. (2022). Crystallization behavior of calcium silicate hydrate in highly alkaline system: Structure and kinetics. *Journal of Crystal Growth*, *584*, 126578. https://doi.org/10.1016/j.jcrysgro.2022.126578.
82. Raponi, A., Romano, S., Battaglia, G., &Buffo, A. (2023).Computational modeling of magnesium hydroxide precipitation and kinetics parameters identification. *Crystal Growth & Design, 23*(9), 6425–6437.https://doi.org/10.1021/acs.cgd.3c00469.
83. Raponi, A., Fida, D., Vicari, F., Cipollina, A., & Marchisio, D. (2025). Computational fluid dynamics and population balance model enhances the smart manufacturing and performance optimization of an innovative precipitation reactor. *Processes, 13*(6), 1721. https://doi.org/10.3390/pr13061721.
84. Romano, S., Trespi, S., Achermann, R., Marchisio, D. L., & Buffo, A. (2023).The role of operating conditions in the precipitation of magnesium hydroxide hexagonal platelets using NaOH solutions.

Crystal Growth & Design, 23(5), 3472–3484.https://doi.org/10.1021/acs.cgd.2c01477.

85. Safarpour, M., Arefi-Oskoui, S., & Khataee, A. (2020). A review on two-dimensional metal oxide and metal hydroxide nanosheets for modification of polymeric membranes. *Journal of Industrial and Engineering Chemistry, 82*, 31–41. https://doi.org/10.1016/j.jiec.2019.11.002.
86. Shen, Y., Wu, Y., Xue, H., Wang, S., & Yin, D. (2021).Insight into the coprecipitation-controlled crystallization reaction for preparing lithium layered oxide cathodes. *ACS Applied Materials & Interfaces, 13*(37), 44163–44173.https://doi.org/10.1021/acsami.1c11849.
87. Siddig, O., Elkatatny, S., & Alafnan, S. (2024). Optimizing hematite filter cake treatment using reducing agents. *Scientific Reports, 14*, 11857. https://doi.org/10.1038/s41598-024-62746-0.
88. Song, L., Li, Z., Wang, G., Tian, Y., & Yang, C. (2021). Supersaturation control of struvite growth by operating pH. *Journal of Molecular Liquids, **336***, 116293. https://doi.org/10.1016/j.molliq.2021.116293
89. Sun, X., Kim, J., & Kim, W.-S. (2021). Spherical agglomeration of nickel–manganese–cobalt hydroxide in turbulent Batchelor vortex flow. *Chemical Engineering Journal, 421*(Part 1), 129924. https://doi.org/10.1016/j.cej.2021.129924.
90. Tang, W., Teng, Z., Zhang, X., Qin, Y., Ran, B., Xu, Z., Yang, Z., Luo, F., Fu, C., & Zhang, J. (2026). Controlled synthesis and mechanistic insights of spherical α-Al_2O_3 nanoparticles for chemical mechanical polishing. *Colloids and Surfaces A: Physicochemical and Engineering Aspects, 741*, 140290. https://doi.org/10.1016/j.colsurfa.2026.140290.
91. Trukhina, M., Popov, K., Oshchepkov, M., Kovaleva, N., & Redchuk, A. (2022). Impact of colloidal iron hydroxide and colloidal silicon dioxide on calcium sulfate crystallization in the presence of antiscalants. *International Journal of Corrosion and Scale Inhibition, 11*(3), 1247–1260. https://doi.org/10.17675/2305-6894-2022-11-3-13.
92. Ventimiglia, L., Vassallo, F., LoBurgio, G., Campione, A., Cammilli, L., Vicario, P., Battaglia, G., Vicari, F., Cipollina, A., Tamburini, A., & Micale, G. (2025). Pilot scale production of $Mg(OH)_2$ compounds from a real industrial reverse osmosis desalination brine. *Desalination, 613*, 119052. https://doi.org/10.1016/j.desal.2025.119052
93. Wang, J., Liu, Y., Feng, L., Wang, Y., & Jia, H. (2022). New insights on UV-activated transformation of polynuclear Fe-hydroxide and iron (III) (hydr) oxide for enhanced removal of natural organic matter by ferrate. *Journal of Water Process Engineering, 49*, 103183. https://doi.org/10.1016/j.jwpe.2022.103183
94. Wang, J., Yin, J., & Kong, X. (2022). Influences of PCE superplasticizers with varied architectures on the formation and morphology of calcium hydroxide crystals. *Cement and Concrete Research, 152*, 106670. https://doi.org/10.1016/j.cemconres.2021.106670.
95. Wang, X., Wei, M., Liu, K., Cui, Y., & Yang, Y. (2024).Particle size of calcium hydroxide prepared by wet digestion: Influencing factors and mechanism. *Crystal Research and Technology, 59*(5), 2300196.https://doi.org/10.1002/crat.202300196
96. Wang, Y., Hu, S., Chen, Y., & Qi, H. (2023). High-efficiency air filter aerogel resembling blood cell with heterogeneous epitaxial growth of zeolitic imidazolate framework-8 anchored on tunicate cellulose nanofibers for integrated air cleaning. *Chemical Engineering Journal, 475*, 146415. https://doi.org/10.1016/j.cej.2023.146415.
97. Wu, W., Chen, S., Wang, S., Wang, X., Zhou, X., Liu, X., Feng, G., Zhang, B., Xing, W., Zuo, M., Cai, Z., He, Z., & Xiang, W. (2025). Micro-structure regulation and evolution of hydroxide precursor for radially aligned Ni-rich cathode with superior performance. *Chemical Engineering Journal, 512*, 162403. https://doi.org/10.1016/j.cej.2025.162403.
98. Xu, X., He, C., & Xia, L. (2026). Applications of solvent-driven crystallization in hydrometallurgy: Current status and future perspectives. *Hydrometallurgy, 242*, 106714. https://doi.org/10.1016/j.hydromet.2026.106714
99. Yang, G., Cheng, Z., Bao, H., Zhang, L., Zhang, H., Jia, H., & Wang, J. (2022). Mechanistic insight of weak magnetic field trigger transformation of amorphous Fe(III)-(oxy)hydroxide for enhanced ferrate (VI) towards selective removal of natural organic matter. *Chemosphere, 303*(Part 2), 134967. https://doi.org/10.1016/j.chemosphere.2022.134967.
100. Yang, Z., Xu, Y., Cai, X., Wu, J., & Wang, J. (2023).Studying properties of pervious concrete containing recycled aggregate loaded with TiO_2/layered double hydroxides and its liquid pollutant purification performance. *Construction and Building Materials, 382*, 131272.https://doi.org/10.1016/j.conbuildmat.2023.131272.
101. Yin, X., Hua, Y., Hao, W., Yang, J., & Gao, Z. (2022). Hierarchical nanocomposites of nickel/iron-layered double hydroxide ultrathin nanosheets strong-coupled with nanocarbon networks for enhanced oxygen evolution reaction. *Electrochimica Acta, 420*, 140455. https://doi.org/10.1016/j.electacta.2022.140455.
102. Zhang, D., Cao, J., Zhang, X., & Zeng, Z. (2022).Modification strategies of layered double hydroxides for superior supercapacitors. *Advanced Energy Materials, 12*(30), 2200793.https://doi.org/10.1002/aenm.202200793.

103. Zhang, L., An, B., Chen, H., Chu, J., Ma, J., Fan, Y., & Wang, Z. (2022). Botryoidal nanolignin channel stabilized ultrasmall PdNP incorporating with filter membrane for enhanced removal of Cr(VI) via synergetic filtration and catalysis. *Separation and Purification Technology, 296*, 121409. https://doi.org/10.1016/j.seppur.2022.121409.
104. Zhang, X., Graham, N., Xu, L., & Yu, W. (2021).The influence of small organic molecules on coagulation from the perspective of hydrolysis competition and crystallization. *Environmental Science & Technology, 55*(12), 8201–8210.https://doi.org/10.1021/acs.est.1c01234.
105. Zhang, Y., Li, B., Liu, J., Han, D., & Rohani, S. (2024).Inhibition of crystal nucleation and growth: A review. *Crystal Growth & Design, 24*(3), 1234–1256.https://doi.org/10.1021/acs.cgd.3c01234.
106. Zhang, W., Zhang, X., Song, Y., Gao, F., & Zhang, Y. (2025). High-entropy layered double hydroxide with advanced structural regulation for electrochemical water splitting. *Chemical Communications, 61*, 7532–7542. https://doi.org/10.1039/D5CC01284H.
107. Zhao, J., Li, B., Wang, A., Ge, W., & Li, W. (2022).Floc formation and growth mechanism during magnesium hydroxide and polyacrylamide coagulation process for reactive orange removal. *Environmental Technology, 43*(18), 2812–2824.https://doi.org/10.1080/09593330.2021.1872809.
108. Zhao, Z., Shu, J., Zeng, X., Chen, M., Deng, Z., Ma, L., Yang, Y., & Wei, H. (2024). Enhanced removal of iron from iron-rich manganese ore leaching solution: A promising strategy by seed-induced precipitation. *Separation and Purification Technology, 336*, 126276. https://doi.org/10.1016/j.seppur.2024.126276
109. Zhou, X., Hong, F. F., Wang, S., Zhao, T., Peng, J., & Zhang, B. (2024).Precision engineering of high-performance Ni-rich layered cathodes with radially aligned microstructure through architectural regulation of precursors. *eScience, 4*(1), 100213.https://doi.org/10.1016/j.esci.2023.100213.
110. Zhu, B., Xu, Z., Ning, Y., Wei, G., & Qu, J. (2023). Managing ammonia–alkali balance to control precursor characteristics in co-precipitation process for enhanced electrochemical performance of nickel-rich cathode materials. *Solid State Sciences, 142*, 107224. https://doi.org/10.1016/j.solidstatesciences.2023.107224
111. Zhu, F., Peng, X., Hu, X., & Kong, L. (2022). Particle release rate strongly affects particle size and settling performance of metal sulfides in acidic wastewater: The role of homogeneous and heterogeneous nucleation. *Journal of Hazardous Materials, 424*, 127561.https://doi.org/10.1016/j.jhazmat.2022.129484
112. Zuo, M., Yu, H., Wang, D., & Fan, L. (2024). Jet cavitation-enhanced hydration method for the preparation of magnesium hydroxide. *Chemical Engineering and Processing - Process Intensification, 205*, 110003. https://doi.org/10.1016/j.cep.2024.110003